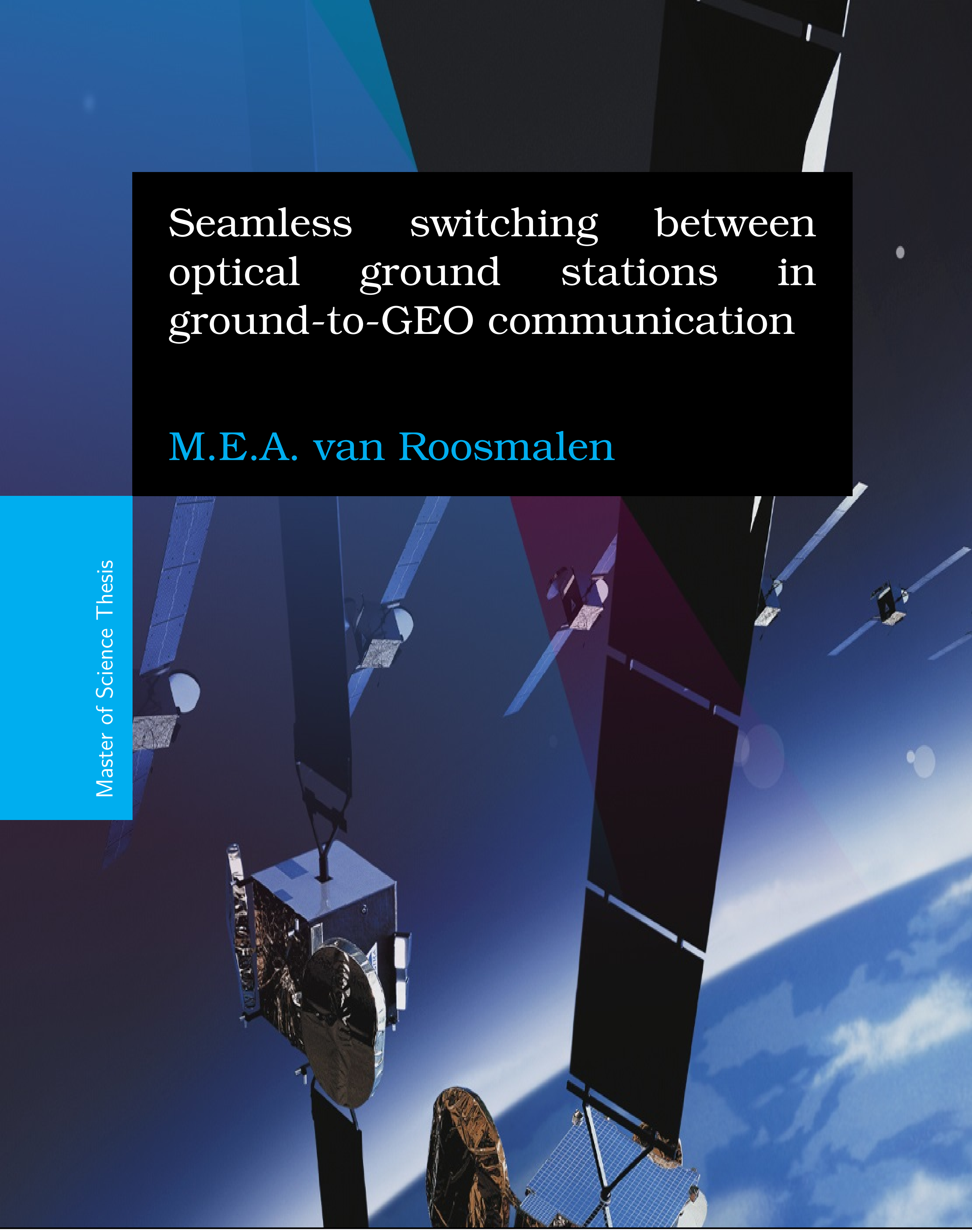

Seamless switching between optical ground stations in ground-to-GEO communication

M.E.A. van Roosmalen

Master of Science Thesis

Delft University of Technology

Delft Center for Systems and Control

Seamless switching between optical ground stations in ground-to-GEO communication

Master of Science Thesis

For the degree of Master of Science in Systems and Control at Delft University of Technology

M.E.A. van Roosmalen

July 25, 2016

Faculty of Mechanical, Maritime and Materials Engineering (3mE) · Delft University of Technology

The work in this thesis was commissioned and supported by SES Techcom Services. Their cooperation is hereby gratefully acknowledged.

Abstract

This thesis discusses the possibility of a seamless switch between optical ground stations (OGSs) in ground-to-GEO communication. First an overview is given of the characteristics of a future optical DVB-S2 feederlink. The equipment at an OGS, the equipment on board of a satellite and the terrestrial network is described along with the effects of the atmosphere on the optical signal.

The objective is to synchronise the signals from two different OGSs towards the satellite. Two existing solutions are presented which do not achieve the required performance. Nevertheless the principle of an existing K_a-band site diversity is promising and is adapted to be used in the proposed solution which uses a fixed delay line combined with a variable photonic delay line (VPDL). The solution is based on the principle of equalising the travelling paths via the two OGSs. To determine the required length of the VPDL a downlink sequence is sent from the satellite to both OGSs and then to a control centre, following the same path as the uplink. The time-delay difference measurement is done on the downlink sequence and used to add a time delay to one of the links.

The performance of several VPDLs are discussed. At the moment of writing this thesis, no existing continuous tunable VPDL meets the requirements of the system. Therefore a system of concatenated switches and delay lines is proposed and tested in simulations.

The satellite movement and the atmospheric turbulences are disturbances on the system that can not be controlled. Predictions of the satellite movement are available, but the turbulences are considered to be purely stochastic. A control strategy is proposed which uses the timing difference measurements on a downlink sequence to control the VPDL, thereby synchronising the OGSs. The measurements are thus done on a parallel feedback system which provides an estimation of the performance metric.

A simulation model is built in *Simulink* containing the signal generation, a switching system, transmission channels for two OGSs and a DVB-S2 receiver. Included in the simulation model is the proposed time delay compensation system. The simulations show the feasibility of the proposed solution. The VPDL will need a precision of a quarter of a symbol time to be seamless. Further tests are necessary to show if the simulation model provides realistic performances.

Table of Contents

List of Figures

List of Tables

Chapter 1

Introduction

Satellite communication has been developed during the second half of the twentieth century [1]. The technology is used to connect different locations on the earth by relaying a communication signal via an artificial satellite flying in an orbit around the earth. The development of commercial satellites is encouraged by the potential of broadcasting one signal from one location and receiving the same signal in multiple locations within the footprint of the satellite. This is very convenient for television broadcasting as connecting more end-users will not increase the cost of the broadcast for the companies. Around the beginning of this century satellite communication also started to be used for internet access. This is especially useful for remote locations which are not connected to the fibre network or for mobile terminals. The global increase of internet demand will therefore also increase the demand for satellite communication.

Most satellite communication nowadays is done via geostationary satellites [2]. A geostationary satellite is considered to stay at the same location above the equator referenced to a point on the earth's surface. As more data is transmitted through geostationary satellites, the demand for usable radio frequencies (RF) has increased to the point that it limits the amount of communication making bandwidth, one of the most valuable resources in satellite communication. Bandwidth determines the data that can be transmitted in a certain time frame. At the moment most communication takes place in the C-band, K_u-band and K_a-band. As the frequencies are limited within these bands and the re-usability of these frequencies is limited due to interference, it is necessary to open other frequency ranges for satellite communications. At the moment one set of frequencies is needed to establish an uplink to a satellite and another set of frequencies is needed for the downlink from the satellites as these may not interfere with each other.

In search for more frequencies different approaches are taken: development of High Throughput Satellites (HTS create multiple small beams in order to reuse the RFs for different location [2]) or using Q/V-band frequencies (Q/V-band are frequencies between 30 and 75 GHz). A third option is to use optical communication which enables the use of a very broad frequency range (100 to 1000 times more than RF) and therefore will be able to transmit large amounts of data [3]. The free space optical frequencies are not regulated by the International Telecommunication Union (ITU) in the same way as the traditional RF bands. Future regulations are not likely as the beams are highly directive and inter satellite interference will be unlikely [3]. This is commercially very attractive. With free space optical communication is meant wireless communication with light that propagates through free space, being air, outer space, vacuum or something similar.

By using optical links for the uplink a whole new range of frequencies can be used which enables more data to be transmitted. As only the downlink has to use the traditional bandwidths, the bandwidth originally allocated to the uplinks can now be reallocated to the downlinks, which doubles the available spectrum. The scenario of using an optical feederlink in the future will be discussed in this thesis. A feederlink is an uplink signal from a ground station to a geostationary satellite which contains all the data intended for one satellite. The wavelength used for optical communications is in the infrared spectrum and will be around 1550 nm. The advantage of the 1550 nm region is that the scattering and absorption for these wavelengths is low [4].

The main disadvantage of using optical links for satellite communications is the link availability. When a cloud blocks the signal from the transmitter on the ground to the receiver on the satellite, the connection will be lost [4]. This is due to the scattering of light on the water droplets in the clouds. An approach to solve this problem is to use multiple optical ground stations (OGSs) from where an optical signal can be transmitted. A possible scenario is shown in Figure 3-1. When a cloud blocks the transmission of a OGS the link can be switched to another location so that the link is kept alive.

To allow a switch between OGSs it will be necessary to have the two uplink signals synchronised at the satellite receivers. This is due to the path length difference of the signals via different OGSs. If the signals are not synchronised, parts of the signal can be lost due to overlapping. It could also be the case that for a short moment in time no signal will be received by any receiver. This will cause an interruption in the signal which can be experienced by end-users. The synchronisation will have to be done every time a switch is done as the path length difference varies due to movements of the satellite and turbulences in the atmosphere.

To overcome the mentioned challenges possible technical solutions will have to be researched to enable the use of optical links in ground-to-GEO communication for commercial use. The technical solutions should require no adaptations on the end-user's equipment. Therefore the solutions will have to allow the use of the widely used Digital Video Broadcasting - Satellite 2nd generation (DVB-S2) standard.

1-1 Goal of the thesis

The main objective of this thesis is to propose technical solutions for seamless switching between OGSs in ground-to-GEO communications. We define seamless switching as changing transmit ground station without interruption in the experience of the end-user.

This objective can be divided into several topics which will be discussed in this thesis.

- What are the general requirements for a ground-to-GEO feederlink?

- What are the specific requirements for seamless switching between ground stations?
- What are the implications for uplink signal time synchronisation?
- Which information is required at which time and place to be able to make the right decisions?
- What techniques can be used to apply the necessary time correction? How can a delay be added to the signal?
- How can the delay line be tuned in order to achieve seamless switching?
- Does a simulation of a switch show the required performance of the system? Will it be possible to achieve a seamless switch?

1-2 Master thesis structure

The master thesis is structured in eight chapters. Chapter 2 defines an optical feederlink and describes the technologies required for such satellite communication. In chapter 3 the point of diversity switching is explained. Also the requirements and limitations for switching OGSs are mentioned. Existing techniques are discussed that are used as an inspiration for the proposed solution. The proposed solution is based on one or more existing techniques which need to be adapted. The expected necessary adaptations and performances are mentioned to conclude the chapter. In chapter 4 an overview of time-delay techniques is given. The different techniques are compared with the requirements for the proposed system and a selection of techniques is made. The chosen control strategy is described in chapter 5. The next two chapters are used to describe the simulation model and discuss the simulation results. The last chapter contains the conclusion and recommendations for further research.

Chapter 2

Optical Feederlink

In this thesis only the uplink from the ground to the geostationary satellite is considered to be optical. This uplink will contain all the data that will be transmitted via the satellite. Such an uplink is called a feederlink as it feeds all the necessary data resources to the satellite. Société Européenne des Satellites (SES) aims at a data throughput of $1\,\mathrm{Tbit\,s^{-1}}$. In the proposed scenario the downlink will still use radio frequencies (RF) as this will not require the end-users to upgrade their equipment and broadcasting can't be done yet with an optical technology. Also the advantage of wider downlink beams to serve television to multiple customers is preserved in RF. A downlink beam is the signal sent from the satellite to the earth. The footprint on the earth of such a beam is typically very large, therefore the same signal can be simultaneously received in multiple locations.

Deutsches Zentrum für Luft- und Raumfahrt (DLR) has already successfully tested an optical link transmitting $1\,\mathrm{Tbit\,s^{-1}}$ from one place on the earth to another in the THRUST experiment [5], which is a test to prepare for an optical feederlink from the ground to a geostationary satellite. In Figure 2-1 an overview of the used feederlink is shown. To reach the high data rate 40 transmission signals of $43\,\mathrm{Gbit\,s^{-1}}$ are wavelength-division multiplexed to constitute one transmission channel. Wavelength-division multiplexing uses different wavelengths to share multiple signals over one medium. The signal multiplexed is amplified by an erbium doped fiber amplifier (EDFA) and optical lenses to give the signal the required gain. On board of the satellite the signal will be received by a detector and demultiplexed. The separate channels are then guided to the corresponding transponders and send down using different RF beams.

2-1 Optical ground station (OGS)

An optical ground station (OGS) is defined as a site on the earth's surface from which an optical signal is sent to a satellite. A data stream enters the station and is led into one or multiple modulators. The data stream is modulated using the Digital Video Broadcasting - Satellite 2nd generation (DVB-S2) standard which is widely used in the industry. Different modulated signals are wavelength division multiplexed to create one signal containing all the

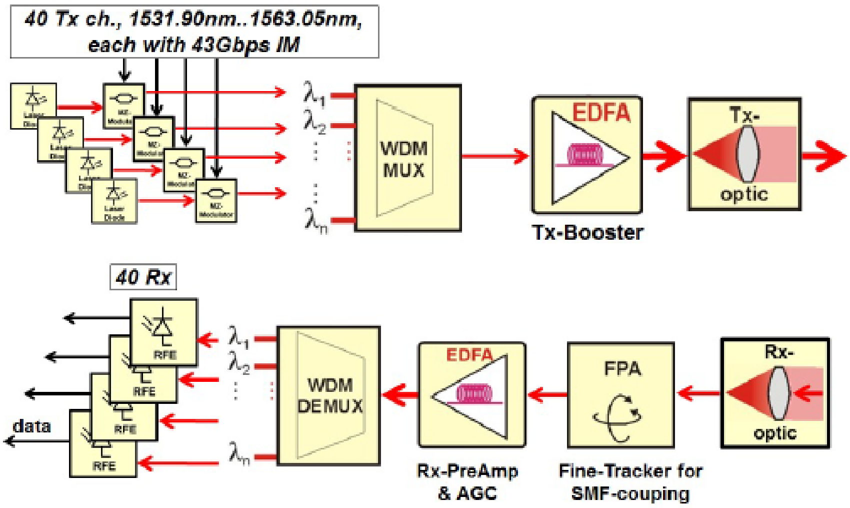

Figure 2-1: An overview for a $1\,\mathrm{Tbit\,s^{-1}}$ optical feederlink as used in the THRUST experiment by DLR. [5]

data intended for the geostationary satellite [6]. The signal is then amplified using an EDFA and sent into the atmosphere by a telescope.

The telescope tracks the satellite using a beacon sent from the satellite. A beacon consists of a light beam which also can be used to send small amounts of data. The telescope is aligned to the received beacon signal using a position sensitive device to measure the angle of arrival. As the telescope is used for both receiving the beacon signal and transmitting the uplink, it is assumed that the transmitted uplink signal will use the same path as the received downlink signal and therefore hit the receiving telescope on the satellite [5]. This is not exactly true as the satellite is moving and the transmitted signal will take around 125 ms to travel to the GEO orbit. This effect is partly compensated as the transmitting beam will be slightly diverging. It still might be necessary to point the beam ahead of the satellites apparent location. When the point ahead angle is larger than the angle of correlating atmospheric turbulence this effect can cause serious pointing errors.

2-2 Satellite payload

The payload of a satellite is defined as the part of the satellite that is used for the main purpose of the satellite. For a communication satellite the payload consists of the parts that handle the signals e.g. receivers, amplifiers, transponders and transmitting antennas. In optical communication, when an optical feederlink signal is received on board of the satellite a telescope and a photodetector are involved.

A signal detection can be coherent or non-coherent. The difference between these two methods is that coherent detection exploits the knowledge of the phase of the signal. Due to atmospheric turbulences the signal will be heavily distorted before being received at the satellite. Therefore the real phase of the transmitted signal will not be known and without use of advanced adaptive optics coherent detection will be impossible. Non coherent detection can be used to receive an on-off keying (OOK) signal. This method represent a one by turning the light on and a zero is represented by turning the light off. A photodetector counts the detected photons and decides if a one or zero is transmitted based on the number of photons detected.

The signal will then have to be converted to a RF signal on board. According to a study performed by SES, there are three approaches to be considered. Each technique has different requirements for the payload.

2-2-1 Transparent

When a transparent payload is implemented the transmitted signal from the OGS will be analogue. This is the same principle as used in RF-over-fiber, but instead of the fiber free space is used as the propagation medium. The optical signal is the modulated DVB-S2 signal, see 2-3. A photo detector at the satellite will convert the light intensity (proportional to the number of photons/s detected) into an electrical amplitude. The signal is then converted to the required downlink frequency and transmitted using RF. This approach is closest related to the existing payloads for satellite using RF. The satellite just acts as a bent pipe and sends the signal back down without altering the signal. This is the most simple approach for the on board system, but will require a high signal-to-noise ratio (SNR). Due to turbulences in the atmosphere it might be difficult to preserve the SNR when travelling through the atmosphere.

2-2-2 Digital transparent

The digital transparent approach adds an A/D converter at the OGS. For this a Δ-modulator is used which tracks the analogue signal by oversampling at 32 times the maximum bandwidth. The digital signal is transmitted using OOK. This technique allows data to be transmitted in a highly attenuated signal without coherency of the phase, [7]. At the satellite the signal can be demodulated using a simple low pass filter, which acts as an integrator. The simplicity of regenerating the signal is an advantage of this approach.

2-2-3 Regenerative payload

Baseband digital data stream is transmitted in this approach. On board the data will be received and modulated into a DVB-S2 carrier. The DVB-S2 signal is thus generated on board and then sent down in RF. Also decisions that are normally made by the modem are required to take place on the satellite. For example the decision of which modulation code will be used for the downlink transmission will have to be done on board. This approach will therefore need processing power to generate the signal, which could be a difficult requirement as will be discussed in section 3-2. Another challenge could lie in the adaptability of the software for new modulation schemes that are yet to be developed during the lifetime of the satellite. Maintenance or firmware updates should be avoided as this will be difficult and costly.

2-3 DVB-S2 standard

DVB-S2 is the standard in satellite communication at the moment. It uses advanced low-density parity-check code (LDPC) to modulate the data stream. The standard is used to make wide variety of modems compatible to the same signal. DVB-S2 is designed by the industry to be used for a variety of purposes [8]:

- broadcasting of standard definition and high-definition TV (SDTV and HDTV);
- interactive services, including Internet access, for consumer applications (for integrated receivers-decoders (IRDs) and personal computers);
- professional applications, such as digital TV contribution and news gathering;
- data content distribution and Internet trunking.

One of the key improvements of DVB-S2 over DVB-S is the use of adaptive coding and modulation (ACM) in point-to-point applications. This features allows optimization of the transmission parameters for each individual user on a frame-by-frame basis. The optimization is done dependent on the path conditions using an closed-loop control via a return channel.

Since 2014 DVB-S2X is released which is an extension to the existing DVB-S2 standard. It adds finer modulation and coding (MODCOD) steps, sharper roll-off filtering, enables bonding of multiple transponders and additional signalling capacity by means of an optional periodic super-frame structure, extended signalling schemes in the header of the physical layer and the support of GSE-Lite signals [9]. In this thesis the extended abilities of DVB-S2X will be assumed as this will be the new standard. In this way, the available RF spectrum is getting exploited closer and closer to the Shannon limits.

2-3-1 Signal structuring

A DVB-S2 signal is structured at the baseband level as a base-band frame (BBFRAME) that consists of the data with an 80 bits header in front, to let the receiver know what modulation codes is used, if the modulated signal consists of one or multiple transport streams or if it is generic data [8]. Both the header and the data are covered by the forward error correction (FEC), which ensures a robust signalling without loss of data. The BBFRAMEs with homogeneous modulation and coding schemes are then collected in physical layer frames (PLFRAMEs) of 64 800 bit with a 90 bit header. The header is used for signalling information and to synchronise the receiver. Receiver synchronisation consists of frame synchronisation, carrier and phase recovery.

Development of super frames (SFRAMEs)

The development of high throughput satellites (HTSs) requires the use of additional signalling for the satellite to support beamhopping. Beamhopping is the term for switching between different downlink beams in HTS. To achieve the additional signalling a new level of frames is added which includes a header with information about the intended downlink beams for the

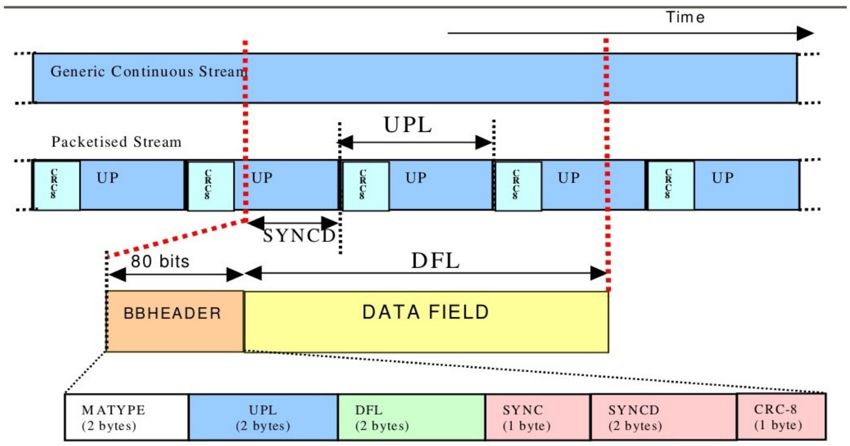

Figure 2-2: Data structure of a DVB-S2 data stream [10].

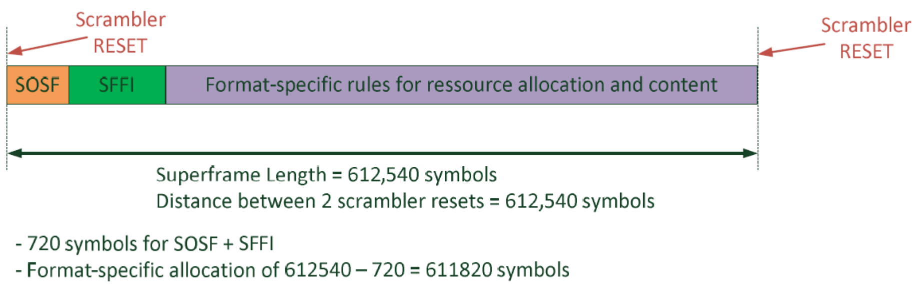

Figure 2-3: Data structure of a SFRAME. The first 720 symbols contain the header. The remaining symbols contain the data structured in PLFRAMEs. [9].

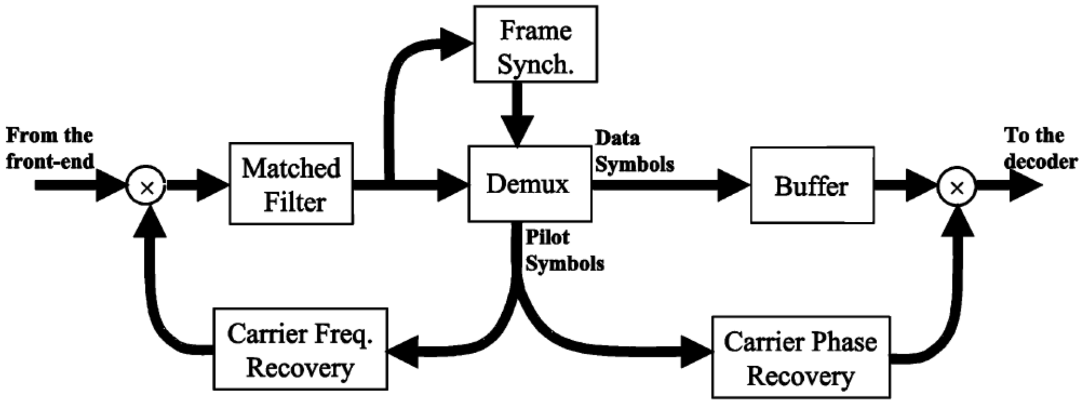

Figure 2-4: A possible scheme for the synchronisation of a DVB-S2 receiver. Synchronisation of the receiver with the signal consist of frame synchronisation, phase and carrier recovery [8].

contained PLFRAMEs[9]. This header could also be used to select the to be used receiver on the satellite. Thereby switching between different uplink locations. There are four structure formats of the SFRAME considered [9]. All proposed structures use a fixed symbol length of frames, being 612,540 symbols. The first 720 symbols contain the header of the SFRAME of which the first 270 symbols contain the start of super frame (SOSF). In this thesis SFRAME structure format 4 is considered as the structure is the most data efficient method. This format uses fixed block sizes of 90 symbols. The blocks contain parts of the PLFRAME. Using this format a PLFRAME can be spread over two SFRAMEs. The use of SFRAMEs enables the possibility to add dummy frames. These frames without containing data can be used as a time buffer to switch from one OGS to another. The advantage is that no valuable data will be lost. In the simulation model the SFRAMEs will not be implemented as the technique is still in development and unsure what choices will be made. To test the performance of the seamless switching the information contained in a SFRAME is not needed.

2-3-2 Synchronisation of the receiver

The synchronisation of a DVB-S2 receiver can be very challenging due to the wide variety of configurations and the low SNR at which it might be operative. It is necessary for the receiver to synchronise with the frames and that the carrier and phase is recovered to be able to demodulate the DVB-S2 signal as shown in Figure 2-4. In the DVB-S2 standard the synchronisation can be divided in a few steps [8]. These are now briefly discussed.

Symbol timing recovery

Symbol timing recovery is done in the acquisition phase to make sure the remote terminals are aligned to same central reference timing signal. A well known technique for this purpose is the Gardner's algorithm, which is non-data-aided and can handle different kind of modulations and frequency errors up to 0.2 times the symbol rate [11]. Acquisitions can be done in 10^5

symbols which corresponds to 2-3 PLFRAMEs [12]. The target performance of the frequency error to lock-in for tracking is assumed to be 5 MHz [8].

Frame synchronisation

The acquisition of frame synchronisation is done by analysing the auto correlation of the pilot symbols in the PLFRAME with the replicas generated at the receiver. The replicas are separated by discrete steps at different taps. The auto correlation of the received signal with the different taps are compared and the maximum auto correlation is selected. It is possible to use a certain auto correlation threshold to select the right symbols represent the start of frame (SOF). A low SNR can be a big problem for frame synchronisation. Frequency offset could also lead to low auto correlation values, therefore a technique called differential post-detection integration can be used.

Coarse carrier frequency recovery

Due to the wide spread market of DVB-S2 modems, the chosen local oscillators are often cheap and thereby of poor quality. This will result in initial frequency offsets up to 5 MHz [12]. Because frame synchronisation is achieved the pilots in the PLFRAME can be used for the frequency recovery. A much used algorithm is Mengali & Morelli, which supports a large pull-in range and performs close to the Cramer-Rao bound [13]. The algorithm uses the following equation to calculate the auto-correlation.

$$R(m) \equiv \frac{1}{N_p - m} \sum_{k=m}^{N_p-1} (r_k d_k)(r^*_{k-m} d^*_{k-m}) \tag{2-1}$$

The results can be improved by averaging the auto correlation values.

$$R(m) = \sum_{i=1}^{M_p-1} R_i(M) \tag{2-2}$$

From this auto-correlation the coarse frequency is estimated as follows.

$$\hat{f}_0 = \frac{1}{2\pi T} \sum_{m=1}^{N} w_m \arg\{R(m)R^*(m-1)\} \tag{2-3}$$

SNR estimation

Estimation of the SNR is important as the result can be sent back to the transmitter to adapt the MODCOD for the link to optimize the throughput. The SNR is also used in the soft demodulation to compute the probabilities of the received symbols. In $\mathrm{K_a}$-band systems it can be assumed that atmospheric attenuation is a very slowly varying process which enables the estimation of the quasi-stationary channel conditions. For optical communications the temporal coherence will be shorter as turbulences in the atmosphere changes the channel conditions faster, see section 2-5.

Fine carrier frequency and phase tracking

Using a second order phase-locked loop (PLL) a finer frequency offset and phase offset is corrected. First a maximum-likelihood (ML) feedforward estimator is applied on a pilot sequence to get an initial estimate for the phase. The estimate is then used to further track the phase and frequency with the second order PLL.

2-4 Microwave photonics

With microwave photonics an RF signal is carried using optical waves. To generate an RF out of the much higher optical frequencies the following principle can be used [14]. Assume we have two optical waves, E_1 and E_2 with angular frequencies ω_1 and ω_2. A typical wavelength used for optical communication has a wavelength around 1550 nm and therefore a frequency of 193.548 THz and a angular frequency of 1215.259 08 rad s^{-1}.

$$E_1(t) = E_{01}\cos(\omega_1 t + \phi_1) \tag{2-4}$$

$$E_2(t) = E_{02}\cos(\omega_2 t + \phi_2) \tag{2-5}$$

With E_{0i} the amplitude of the waves and ϕ_i the phase terms. When these two signal are coupled this results in the following signal.

$$I_{RF}(t) = A\cos((\omega_1 - \omega_2)t + (\phi_1 - \phi_2)) \tag{2-6}$$

I_{RF} is the RF signal and A is the constant representing the amplitude of the signal as a result of E_1 and E_2. Due to the bandwidth limitations of the photo detector only the term shown in equation 2-6 will be received. This term represent the RF signal and as shown can have a much lower frequency (MHz/GHz) as the optical waves(THz).

For controlling the amplitude of a light wave containing the RF signal a Mach-Zehnder modulator can be used. This device consists of a beam splitter which divides the laser light in two different paths. One of the paths contains a phase modulator which alters the phase of the wave. When the two signals are recombined the interference of the two beams can be constructive or destructive depending on the control of the phase modulator. As a result the amplitude or intensity of the exiting light can be altered [15].

Dense wavelength-division multiplexing (DWDM)

A widely used technique to transport large amounts of data over fiber in the terrestrial network is dense wavelength-division multiplexing (DWDM) [16]. As the name suggests different channels are separated by using different wavelengths. These channels are often indicated as different colours of light, even though the wavelengths are centred around 1550 nm and thus not within the visible spectrum. In dense WDM the channels are packed very close together opposed to coarse WDM which uses certain guard bandwidths to prevent inter-channel interference. A typical DWDM system holds 40 channels with a spacing of 100 GHz between them [17]. One channel can achieve a bitrate up to 43 Gbit s^{-1}. So theoretically a single DWDM system can provide a bitrate of 1.6 Tbit s^{-1} which is sufficient for the proposed

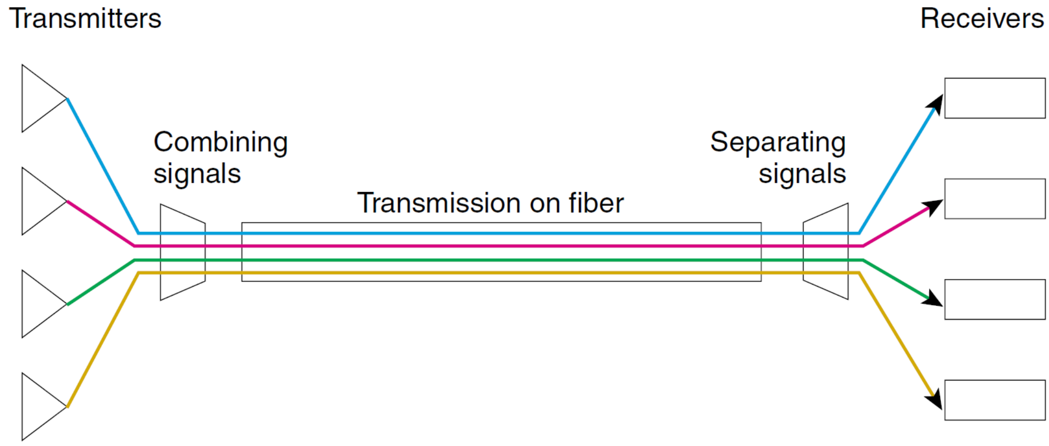

Figure 2-5: The principle of DWDM explained [16].

system. At the moment already channel bitrates of 100 Gbit s^{-1} are being researched and developed to further increase the capacity of DWDM. The transmission can also be used in both ways and is therefore bi-directional.

The signal will be sent over DWDM in L-band frequencies which are between 1 and 2 GHz. The wavelengths used for L-band in optical communication are in the range of 1571 nm and 1611 nm. This choice is made for practical reasons as the use of L-band is common within telecommunication.

DWDM can be used over long distances, but this will lead to deterioration of the signal. The deterioration can be divided in to several effects being attenuation-decay of signal strength, chromatic dispersion and nonlinearity-cumulative effects as a result of interactions with the material it propagates through [16].

Attenuation can be divided into Rayleigh scattering and absorption. Rayleigh scattering is a result of small variations in the material that are smaller than the wavelength of the light. Absorption is caused by impurities in the material and decreases the transmitted intensity of the light. To ensure the SNR at the receiver for long range DWDM it is necessary to use repeaters placed approximately every 100 km to amplify the signal.

Dispersion is the spreading of light pulses as it travels through optical fiber. These distortions of the signal limits the bandwidth of the signal. Chromatic dispersion is linear and polarization mode dispersion is nonlinear. Chromatic dispersion is a result of different travelling speeds for light with different wavelengths. The increase of the effect of chromatic dispersion is as the square of the bitrate. The use of single mode fiber (SMF) retains the fidelity over long distances better than multimode fiber. This is due to a very small core which reduces the dispersion.

The nonlinear effects in DWDM exist of stimulated Brillouin scattering, stimulated Raman scattering, self-phase modulation, and four-wave mixing. The four-wave mixing is the most prominent in DWDM technology. This is caused by third order nonlinear interactions among different DWDM channels which create sidebands that can cause interchannel interference. The interaction of three channels can produce a fourth frequency which result in cross talk

Symbol	Description
A_f	peak amplitude of the Gaussian pulse of channel f
a_{fk}	modulating symbol of channel f and pulse k
T_s	symbol period
Φ_{fk}	phase of pulse k in channel f

Table 2-1: Parameters used in the signal propagation model.

and SNR degradation.

The propagation of the signal through SMF can be described by the following nonlinear Schrödinger (NLS) equation [18]

$$\frac{\partial A}{\partial z} = -\frac{\alpha}{2}A - \frac{i\beta_2}{2}\frac{\partial^2 A}{\partial t'^2} + i\gamma|A|^2 A \tag{2-7}$$

Where A is the slowly varying complex envelope of the propagating field is, t' is measured in the frame of reference of the moving pulses at group velocity v_g and the propagated distance is represented by z. The three terms on the right hand side describe respectively the attenuation, dispersion and nonlinearities on the pulses in the fiber. With α the attenuation constant per km, β_2 the group velocity dispersion and γ the nonlinear parameter. The transfer function for a signal propagating through fiber in the frequency domain can then be described by [18]

$$H_1(\omega, L) = \exp\left(-\frac{\alpha}{2}L + i\frac{\beta_2}{2}\omega^2 L\right). \tag{2-8}$$

Where L is the length of the fiber. The signal input in the fiber is denoted by $S(\omega)$ [18].

$$S(\omega) = \sqrt{2\pi}\sum_{f=0}^{F-1}\sum_{k=0}^{K-1} a_{fk}A_f\tilde{T}_f \times \exp\left[-\frac{(\omega - f\Delta)^2\tilde{T}_f^2}{2} - i(\omega - f\Delta)KT_s + i\Phi_{fk}\right] \tag{2-9}$$

With F the number of equally spaced channels, K consecutive Gaussian pulses and Δ the channel spacing. The remainder of the parameters are described in Table 2-1.

Besides the described effects in this section the signal is also effected by the used amplifiers, detectors and other equipment. These effects depend on the choices made in the system design.

2-5 Atmospheric propagation

The biggest effect on the signal towards the satellite is the travelled distance through the atmosphere. The atmosphere is defined as the layer of gasses around the earth. The propagation through the first 1000 km of the atmosphere is difficult to predict due to turbulences. The index-of-refraction turbulences (IRT) result in different effects. For uplink beams the scintillation and beam wander have the most effect on the performance of the signal [19]. Scintillation can be seen as the twinkling of stars. The scintillations are a result of small eddies formed in the atmosphere. An eddy is a swirling motion of the air due to turbulences. The larger eddies which are crossed by the entire beam cause refractions and deviates the beam slightly from it's path. The difference of direction at the exit of the atmosphere results in wandering of the beam.

The atmosphere and thus the channel of the signal changes constantly due to the turbulences. The channel coherence time, τ_c is considered to be the time period over which the channel can be seen as constant. Typical values for τ_c for atmospheric channels to fixed terminals are 2 ms to 50 ms [20].

Assumed is that a collimated beam is transmitted from the ground to a geostationary satellite. The profile of the beam in the long term is Gaussian and the width of the beam is defined as the width for which the electric field decays by $1/e$ with respect to the maximum in the centre of the beam.

2-5-1 Scintillation

The intensity field is an ergodic process, therefore the scintillation intensity index σ_I^2 is expressed as the variance defined as follows.

$$\sigma_I^2 = \frac{\langle I^2(L,x,y,t)\rangle - \langle I(L,x,y,t)\rangle^2}{\langle I(L,x,y,t)\rangle^2} \tag{2-10}$$

With the intensity I depended of the channel distance L, the transverse coordinates x, y and time t. For the on-axis scintillation the following expression can be used for the Rytov variance[20].

$$\sigma_R^2 = 2.25k^{7/6}\int_0^L C_n^2(z)\cdot(L-z)^{5/6}\,\mathrm{d}z \tag{2-11}$$

$$\text{For } C_n^2 = \text{const} \tag{2-12}$$

$$\sigma_R^2 = 1.23C_n^2 k^{7/6}L^{11/6}, \quad k = \frac{2\pi}{\lambda} \tag{2-13}$$

With C_n^2 is the index-of-refraction structure constant. For weak turbulences ($\sigma_R^2 < 0.5$) the values are similar to σ_I^2. This is also true for strong turbulences where the values drop to the saturation level. The biggest discrepancy is around the peak values for medium turbulences ($\sigma_R^2 \approx 2.8$).

To evaluate the results for received signal the received optical power $P_{Rx}(t)$ is used. $P_{Rx}(t)$ is the time-dependent integral of $I(x,y,t)$ over the receiver aperture A_{Rx}. Lognormal behaviour of the received power is a good approximation in all turbulence cases weak, intermediate, strong and saturation when some amount of aperture averaging takes place [21].

2-5-2 Beam wander

In uplink optical communication beam wander has a large effect as the signal intensity at the receiver on the satellite can heavily vary as a result. Beam wander results in random displacements of the centre of the beam along the coordinates x and y. β_x and β_y are normal random variables according to [22]. The absolute displacement is then defined as follows.

$$\beta = \sqrt{\beta_x^2 + \beta_y^2} \tag{2-14}$$

$$\langle\beta_x^2\rangle = \langle\beta_y^2\rangle = {}^1\!/\!{}_2\langle\beta^2\rangle \tag{2-15}$$

The variance of the displacement can be expressed assuming the beam maintains its Gaussian profile and the turbulence is weak [23]

$$\langle\beta_x^2\rangle = 2.07\int_0^L C_n^2(z)\cdot(L-z)^2\left[\frac{1}{W_s(z)}\right]^{1/3}\mathrm{d}z \tag{2-16}$$

With $W_s(z)$ the short term beam width.

2-5-3 Detection of on-off keying (OOK) in turbulence channels

To simulate the effect of the atmospheric turbulences on the received signal some assumptions will have to be made. The SNR is limited by shot noise of ambient light, which can be correctly modelled as white Gaussian noise [24]. We define T as the bit interval of the OOK and we assume that the received photocurrent is integrated by the detector over an interval $T_0 \leq T$. During a bit the channel is assumed to be constant as $T \ll \tau_c$ The received electrical current can than be expressed as follows:

$$r_e = \eta(I_s + I_b) + n, \tag{2-17}$$

with I_b the intensity of the ambient light and n is additive white noise [24]. I_s is the signal intensity and will be zero for an off bit and a certain constant for an on bit. The optical to electric conversion constant is calculated as

$$\eta = \gamma T_0\cdot\frac{e\lambda}{hc}. \tag{2-18}$$

γ describes the efficiency of the photodetector, e is the electrical charge, λ the wavelength of the received signal, h is Planck's constant and c is the speed of light. Subtracting the the electric power as a result from the ambient light γI_b will result in the following probability densities for the on or off bit respectively [24],

$$P(r|\text{off}) = \frac{1}{\sqrt{2\pi\sigma_R^2}}\cdot\exp\left(\frac{-r^2}{2\sigma_R^2}\right) \tag{2-19}$$

$$P(r|\text{on}) = \int_{-\infty}^{\infty}\frac{1}{\sqrt{2\pi\sigma_R^2}}\cdot F_X(X)\cdot\exp\left(-\frac{(r-\eta I_0 e^{2X-2\mathrm{E}[X]})^2}{2\sigma_R^2}\right)dX \tag{2-20}$$

With X the log-amplitude fluctuation of the signal and $F_X(X)$ is its Gaussian marginal distribution.

The detection of the bits can then be done in several ways. Due to the variations of the signal strength as described in the previous sections it will be important to interpret the received photons in a good manner. A threshold can be used to acknowledge the receiving of an on or off bit [20]. Also a symbol-by symbol ML method can be used which looks at the probability densities of receiving an on or off bit. A more advanced technique uses a sequence of bits which thereby acquires knowledge of the turbulences in the atmosphere [24].

Chapter 3

Site diversity

The main challenge for ground-to-GEO optical satellite communication is high attenuation of the signal due to clouds. Every time a cloud will move between the optical ground station (OGS) and satellite the link will be blocked. To provide commercially viable communication services it will be necessary to ensure a link availability of more than 99.999% according to SES. This means only an outage of a few minutes per year is allowed. To improve link availability multiple transmission sites will be used. This principle of using a variety of ground stations to improve link availability is called site diversity.

The advantage of multiple ground stations can be explained as follows. When the signal of OGS #1 will be blocked by a cloud the signal will be switch to OGS #2 which has clear sky conditions. This scenario is depicted in Figure 3-1. To ensure link availability it will be necessary to use a network of OGSs to make sure there is always one location with clear sky conditions. The use of diverse transmission sites for one satellite link to ensure link availability is called site diversity. The number of necessary OGSs is researched by Deutsches Zentrum für Luft- und Raumfahrt (DLR) in [25]. To ensure a 99.999% link availability a network of at least 8 OGSs will be necessary. This number will dependent on the locations of the OGSs. The locations are therefore strategically chosen and spread over an intercontinental network. The correlation of cloud coverage for different locations should be taken into account. The maximum distance between OGSs within a future network is approximately 10 000 km. If a network with a smaller spread will be used, the number of OGSs will have to be increased.

For this approach a control centre will be needed to decide which OGS is used for the feederlink. The decision can be made based on weather prediction models to limit the number of switches to a minimum. The number of switches needed per year will be dependent on the design of the network. According to first estimations it will be necessary to switch approximately 500 times a year.

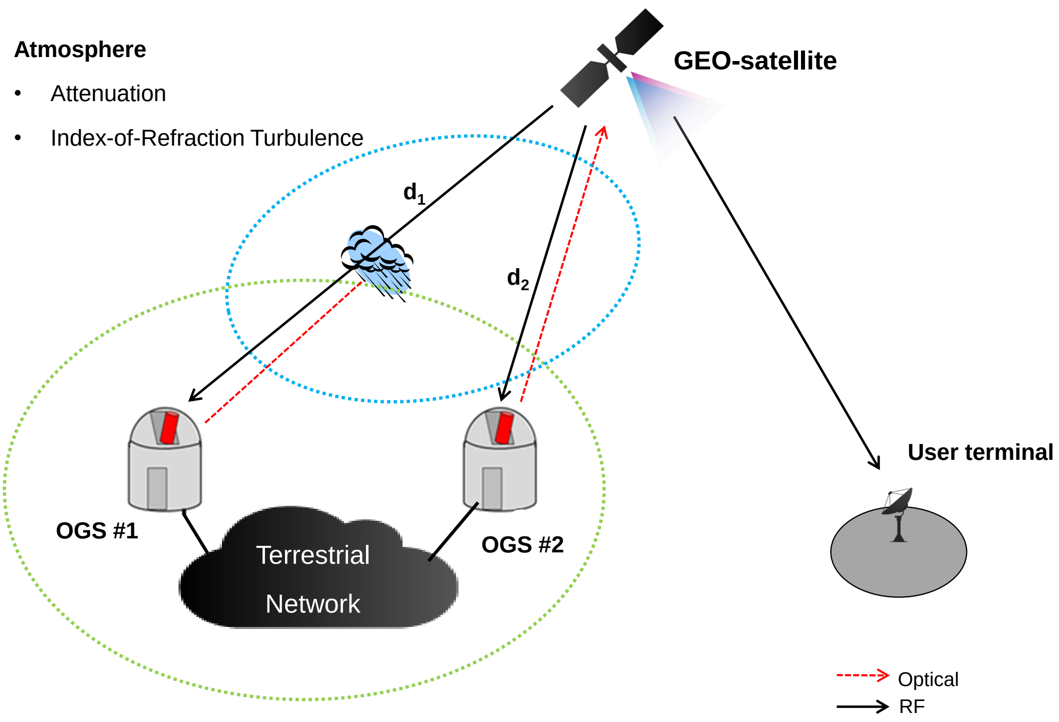

Figure 3-1: A possible scenario to deal with the limited link availability of an optical link caused by weather systems. When the optical pathway of OGS #1 is blocked it will be necessary to switch to OGS #2. d_1 and d_2 are the distances from the OGSs to the satellite.

3-1 Model definition

To describe the problem, we define the following model. The received signal at the satellite $r(t)$ is expressed in combination of the transmitted signals from OGS #1 and OGS #2.

$$r(t) = a_1(t - \Delta t_1)s(t - \Delta t_1) + a_2(t - \Delta t_2)s(t - \Delta t_2) \tag{3-1}$$

With $a_i(t)$ the amplitude of the signal from the different OGS and Δt_i the time travelled from the OGS to the satellite. The travelled time can be calculated using the speed of light and the distances of the transmitters to the satellite. The distances d_i are defined as shown in Figure 3-1. In this expression we assume no fading of the signals and no added noise. In practice two signals modulated by different modems are not exactly the same. This is a challenge that will be discussed later in this chapter. For now it is assumed that the signals transmitted at the two OGS are exactly the same.

When only OGS #1 is transmitting, $a_2(t)$ will be zero and the satellite will receive the signal from OGS #1 with a certain delay. When a cloud is formed which blocks the signal from OGS #1 it will become necessary to switch. We define the moment of switching as t_0. This decision will be made by some kind of system using weather predictions, which will not be discussed in this research. We assume that both stations still have a clear sky at t_0. OGS #1 will stop sending and a_1 will become 0 after $t = t_0 + \Delta t_1$. At the same moment OGS #2 will start sending and at $t = t_0 + \Delta t_2$ the signal will be received at the satellite as $a_2(t_0) = 1$. Because of the different delays of the signals a certain part of the signal could be lost. If the distance d_1 is longer than d_2 there will be a moment at which the satellite receives both signals. This will cause signal interruption due to interference. If d_2 is longer than d_1 there will be a moment in time at which the satellite does not receive a signal at all.

These problems could be solved by adding a delay to one of the two signals. Often this is done by adding a small buffer at the receiver end which can be used to synchronise multiple signals. Due to several difficulties, it will not be attractive to do this in this situation as the receiver will be on the satellite. Therefore it is necessary to add a delay, t_a at the OGS. Ideally the delay is the same as the delay difference of the two signals. The received signal is then expressed as follows:

$$r(t) = a_1(t - \Delta t_1)s(t - \Delta t_1) + a_2(t - \Delta t_2 - \Delta t_a)s(t - \Delta t_2 - t_a) \tag{3-2}$$

With $t_a = t_1 - t_2$ in the case that d_1 is longer than d_2. When a switch is made the receiver will start receiving the signal from OGS #2 at the precise moment it stops receiving from OGS #1.

Unfortunately this approach will only work when there are no turbulences in the atmosphere and the location of the satellite is exactly known. The turbulences can lengthen the travelling path by refractions in the sky. The location of the GEO satellite differs in time as it moves around in a box of 150 km by 150 km. Movement speed of the satellite referenced to the earth is typically a few meters per second as discussed in section 3-2-1. The variance of the difference between the distances d_1 and d_2 will therefore be in the order of 10 meter per 15 minutes. To account for these effects the model can be extended by assuming $\Delta t_i(t)$ to be variant in time. As a result will the artificially added delay will also be variable. Because of the accuracy limitations of the delay time it might be necessary to add a guard time for switching to ensure no overlapping of the two signals. The propagation speed of light travelling through the atmosphere can also vary due to scattering. The effect of scattering on the propagation delay will have to be investigated. Fading in the atmosphere can alter the signal which makes it more prone to errors, especially when switching. The receiver will have to correct for the different distortions of the two signals. Using channel state information (CSI) predictions of the channel transfer functions can be made, which can be used to correctly interpret the signal. The estimation can be done by using pilot symbols. These are sequences known to the receiver. A processor will compare the known sequence with the received signal and use this to estimate the transfer function. This transfer function can then be used to recover the sent signal $s(t)$ from $r(t)$. One of the major difficulties of the objective situation is that there will be no processing power on board of the satellite to use advanced techniques. Another problem will be the major delay of the feedback to the transmitter. It will take about 125 ms for the signal to go from the transmitter to the receiver, the feedback loop will therefore be more than 250 ms. Because of the delay it might not only be necessary to estimate the channel characteristics but also to make a prediction of the transfer function.

3-2 Satellite properties

Equipment on-board of a satellite has very different requirements from equipment on the ground. This is due to the characteristics of the space were the satellite has to operate and due to the large expenses for a satellite launch. After launch a satellite will be brought in to a geostationary orbit and will have to work continuously until the end of its lifetime. To keep the satellite inside the designated orbit it will need fuel to adjust the position. This is necessary due to other objects in space which can deposition the satellite by their gravitational pull. The amount of fuel on board of a satellite is limited as the added weight will increase the power necessary to launch the satellite into space. For this reason it is desirable to keep the weight of the equipment on the satellite as low as possible. The launch of a satellite can cost several hundreds of millions dollar. Therefore it is important that the satellite will work reliably for the planned lifespan as launch a replacement is expensive. The typical lifespan of a modern geostationary satellite is 15 years.

The power needed for operating the satellite will have to be generated in space as it will impossible to transfer it to space. Solar panels are an attractive solution as the energy production is predictable in space where no atmosphere can block the sunlight. Even though the produced power can be predicted it is still limited. The power usage is also limited due to the lack of atmosphere. When processing power is used, heat will be generated. As there is no air in space no convection can take place to dispose of the heat. The high temperature can then result in system failures. When the system breaks down it is very difficult to repair or replace parts of the satellite as the satellite is 36 000 km away. The used parts must therefore be very reliable and often satellites are equipped with redundant parts. As this will add weight to the satellite, only crucial parts will have redundancy.

The use of software should be avoided at a satellite. Software can be corrupted, which can cause a failure of the system and thereby lose control of the satellite. If software needs to be updated due to technological developments, problems can occur. The risk of corruption during the firmware update is best to be avoided.

3-2-1 Satellite movement

A geostationary satellite is in an orbit at an altitude of approximately 36 000 km directly over the equator. One rotation of the satellite around the earth takes exactly 24 h, as the angular velocity is the same as the earth rotating around its axis. Therefore the satellite is always above the same point on the earth's surface and seems to be stationary to an observer on the ground.

Due to gravitational attraction from other objects in space the satellite will have small deviations from its orbit. Some steering control is needed to compensate for these deviations. Typically the satellite is kept within a box of 100 by 100 km. The movement of the satellite within the box, as seen from an observer at the ground station is typically best described by a figure of eight. As a result the path length between the ground station and the satellite differs. The speed of the satellite in respect to the earth is only a few $\mathrm{m\,s^{-1}}$ [26]. As the path length changes gradually this is normally no problem for the signal receiver.

When multiple ground stations are assumed in a system. The relative path length difference can be significant. For example we look at the ASTRA 4B satellite which is positioned at

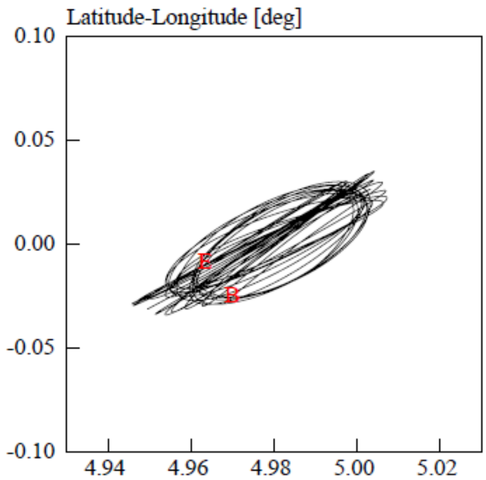

Figure 3-2: Lattitudal and longitudinal movement of the ASTRA 4B satellite at $4.98°$. The red E's show the position of the satellite at the moment of performing an East-West correcting manoeuvre. [26]

longitude 4.98° East. The path length difference from the satellite to the ground station in Gibraltar and from the satellite to the ground station in Agesta (Sweden) is approximately 2075 km. The signal path lengths are defined as d_1 and d_2 in Figure 3-1 In a direct line on earth the two ground stations are 3075 km apart. Due to the movement of the satellite in the box, as seen in Figure 3-2, the relative path length difference from the two ground stations to the satellite can vary up to 3468 m. As switching between two OGSs is investigated in this thesis, it is important to compensate for this varying path length difference.

3-3 Existing seamless switching techniques

Site diversity for link availability is needed for optical communications but not exclusively. Also in K_a-band it can be necessary to use multiple transmission stations to ensure link availability. This is because the K_a-band is in higher frequencies and therefore more affected by weather. Therefore there exists a switching solution provided by DEV systemtechnik [27]. This solution uses one single modem and recreates two similar links for switching. The signal is transmitted using dense wavelength-division multiplexing (DWDM) over fiber [27]. In terrestrial networks there is already equipment capable of seamless switching between two signals. To achieve a seamless switch the two signals are monitored simultaneously and are processed into one new transport stream (TS). The seamless switching equipment manufactured by Nevion can handle MPEG-2 transport streams. In this chapter the two mentioned approaches will be discussed and compared. This comparison is then used to decide on the further research.

3-3-1 Seamless TS Monitoring Switch

At the moment there are a few seamless TS monitoring switching systems on the market. The principle used for this system is to monitor both the links at the receiver. A processor than analyses the stream and the received data packets counter will be read. Behind the receivers a small buffer will allow the system to delay some of the packets. If packets #1 and #2 are received through the first link and within the allowed buffer time packet #3 through the second link, the processor will know this and stitches the packets together in the right order and thereby creates a seamless switch. This approach works while the processor can read the packet counter. When the transport stream will be modulated in a DVB-S2 signal, the receiver will need to demodulate the signal before the packet counter can be read.

To work for a feederlink it will have to be adapted to work with a DVB-S2 demodulator. In a study of S. Cioni in 2007 [28] the problem is researched for a satellite communication system designed for railway systems. In their case the DVB-S2 modulation is already implemented by means of demodulators. This approach is possible as there are no limitations on the power supply in the railway system and the signal does not have to be remodulated. For implementation on the satellite this could be a problem as the processing power needed for this equipment will not be available on board of the satellite. The limiting factors as electrical power and the lack of proper cooling techniques in space are discussed in section 3-2

3-3-2 K_a-band site diversity

In some existing K_a-band time division multiple access (TDMA) networks diversity switching is applied. TDMA networks connect multiple remote locations to one hub station. For all the links the same bandwidth is shared in time. The hub station provides the remote locations with the requested data in short time bursts. The remote locations know which time slots are allocated to them and thereby know which data to collect and when to transmit data to the hub without data overlapping with data from other remote locations. If the location of the hub station suddenly is changed the synchronisation between the allocated time slots ceases to exist because the travelling time of the signal will be changed. Therefore the following approach is used to achieve seamless switching in a TDMA network. In this approach it is attempted to create two identical signal paths over which the same signal is sent. One of the key points is that this technique uses only one modulator at a control centre instead of a modulator at each transmitter station. Different modulators without proper synchronisation will end up in different modulated signals as the frequency and timing are different for each device.

In Figure 3-3 a schematic version of the setup is shown [27]. The signal from the modulator is sent using DWDM (2-4) to the main transmitter station and a back up transmitter location within 100 km is also connected to the modulator. To compensate for the difference in optical path length between the modulator and the satellite an optical delay line is added to path of the main transmitter, thereby equalizing the distance and thus time travelled of the signal from the modem to the satellite. The length of the optical delay line is fixed and can be set with discrete steps of 10 ns for the compensation of the path length difference. Even though the path length difference varies continuously due to movements of the GEO satellite this causes no interruption in the signal. This is due to the use for TDMA networks. Because the synchronisation between multiple ground stations (up to 1000 stations) is difficult, TDMA networks add certain guard times before and after the designated time slots. Therefore the system is robust and can handle variations in path length depending on the size of the guard times.

A fast radio frequencies (RF) switch is connected to the modem, which switches the path way of the signal from the main antenna site to the diverse antenna site in negligible time. As the path lengths are the same the signal from the diverse antenna site will be received as soon as the satellite stops receiving the signal from the main antenna site. This is how the seamless switch is achieved.

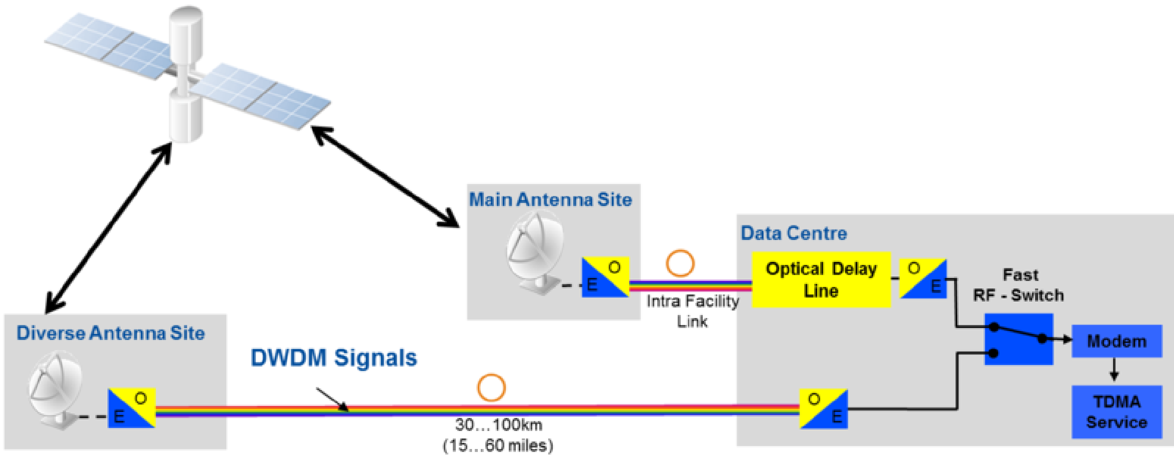

Figure 3-3: A solution provided by DEV systemtechnik to provide K_a-band site diversity for TDMA networks. By making sure the path length of the signal, from the modem to the satellite, is equal for both the transmitter locations a seamless switch is achieved. [27]

3-4 Proposed solution

To solve the problem of seamless switching for optical feederlinks the same principal as in the K_a band switching by DEV is used. One modulator is based at the control centre. The modulated signal is sent to the two OGSs using DWDM. From there the pathway will be in free space towards the satellite. This enables the use of the model proposed in section 3-1. For this the model of the received signal on the satellite has to be extended to the control centre.

$$r(t) = a_1(t - \Delta t_1 - t_a)s(t - \Delta t_1 - t_a) + a_2(t - \Delta t_2)s(t - \Delta t_2) \tag{3-3}$$

$$\Delta t_i = \Delta t_{ti} + \Delta t_{fi} \text{ , with } \ t_{ti} = d_{ti}/c_t \text{ and } \ t_{fi} = d_{fi}/c_f \tag{3-4}$$

$$\epsilon = \Delta t_2 - (\Delta t_1 + t_a) \tag{3-5}$$

Δt_1 is defined as the total travelling time of the signal from the control centre to the satellite. This is a combination of the time travelled through the terrestrial fiber, Δt_{t1}, and the time travelled through free space Δt_{f1}.

To make sure the signals reach the satellite at the same time a delay line is added. The necessary length of the delay time has to be estimated. To do this a simple downlink sequence

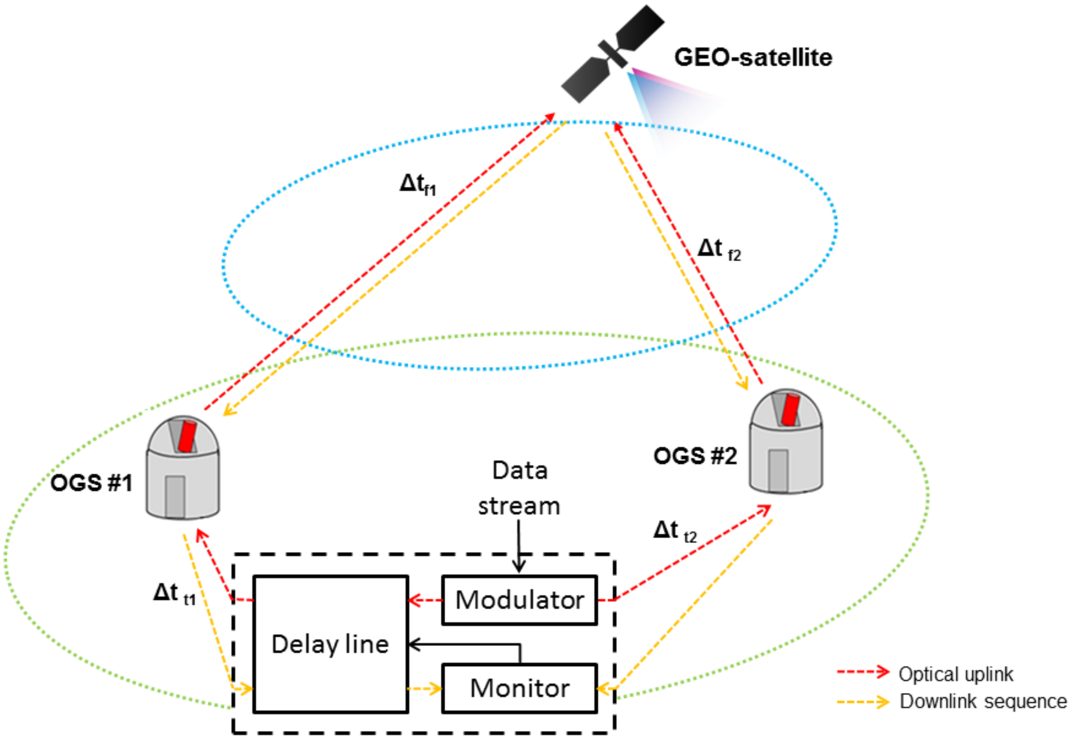

Figure 3-4: The suggested solution for switching between OGSs for a feederlink. By making sure the path length of the signal, from the modem to the satellite, is equal for both the transmitter locations a seamless switch is achieved. This is done by synchronising a sequence sent from the satellite down through the two optical links.

is sent from the satellite to the OGSs using the tracking beacon, as described in section 2-1. The sequence will travel the same optical path as the uplink, but in the opposite direction. Therefore the travelled distance is assumed to be the same as the uplink signal. At the control centre a device will monitor the downlink sequences of both travelled paths and compare the time of arrival.

$$\hat{\epsilon} = \Delta t_{2d} - (\Delta t_{1d} + t_a), \tag{3-6}$$

with t_{1d} being the travelling time of the downlink signal via OGS #1 and t_{1d} via OGS #2. The estimated difference is then used to adjust the length of the delay line. Using a controller the received sequences can be synchronised at the monitor. This adjustment of the delay line will influence the path length in both directions. As it is assumed that the travelled path for the uplink is the same as for the downlink sequence the signals of OGS #1 and #2 will now be synchronised at the satellite. The measurements of the timing difference are thus done on a parallel system. The downlink sequence will therefore act as an estimator for the performance of the uplink signal. The disturbances will act in the same way on the original and the parallel system. The parameters used in the system are shown in Table 3-1.

In this approach some points are neglected to simplify the solution. The paths in opposite

Controllable parameter	t_a	Time added by the variable delay line
	a_1, a_2	Amplitude of the signals
Model parameters	$\Delta t_1, \Delta t_2$	Travelling times to the satellite, dependent on satellite movement and atmospheric turbulences
Output	$\hat{\epsilon}$	Difference between travelling times including the delay line, it is an estimation as it is measured for the downlink path

Table 3-1: Parameters of the proposed system.

directions might not be exactly the same. This is especially true for the free space part due to turbulences. Path lengths will also be different as a result of the moving satellite. The delay line length will be adjusted based on the received signal which left the satellite ∼125 ms before. The adjustment will influence the uplink signal that will arrive ∼125 ms later at the satellite. This total delay of ∼250 ms might cause a difference in path lengths and therefore cause an interruption in the signal.

The CSI estimation of the atmosphere can be done using the downlink sequence. The correlation of two signals propagating in opposite directions through the same medium is quite high. Experiments showed a correlation of 0.993 for bidirectional free space optical communication over a distance of 7 km [29]. Therefore it is expected to be valid to use the timing of the downlink signals for the uplink as the atmosphere is considered to be constant for a short coherence time, τ_c as described in section 2-5. The time of the downlink sequence entering the most turbulent part of the atmosphere and the uplink leaving that part of the atmosphere is shorter than the temporal optical coherence which varies between 2 ms and 50 ms.

For seamless switching it is necessary that the satellite is equipped with at least two telescopes which can be pointed independently. This requirement is necessary as one telescope will not be able to receive the signal from two different OGSs at the same time. For seamless switching the repointing to another OGS will have to happen instantly which is theoretically impossible through mechanical means. When multiple telescopes are used it will be possible to repoint one of the telescopes to the next OGS before the switch is made. To control the actions of the satellite a certain control signal will have to be sent up. The requirements for this uplink are not very strict as only a small amount of data is needed and the switching scheme does not need to be constantly updated.

Chapter 4

Optical delay lines

To compensate the path length difference from the modulator to the satellite via both optical ground stations (OGSs) a delay line will be needed. For a delay line a simple optical single mode fiber (SMF) can be used. The fiber can be wound on a spool to reduce the volume of the device. The delay line will compensate the coarse difference with a fixed delay which can go up to a few 1000 km [26] for the planned network crossing continents based on the research done in [30]. The necessary delay goes up to the order of magnitude of $\sim$10 ms. A delay line is designed to cope with a wide bandwidth to reduce dispersion of the different wavelength channels as used in dense wavelength-division multiplexing (DWDM) and described in section 2-4. To preserve the signal-to-noise ratio (SNR) it will be necessary to use signal repeaters every 100 km.

The satellite moves within a fictional box in the geostationary orbit as described in section 3-2-1. This results in a variance in the path length difference between OGS that can be as large as a few kilometres. which can result in a receiving delay of $\sim$10 µs [26]. As this difference changes constantly it is necessary to add a variable photonic delay line (VPDL) to the system. A variable delay can be achieved with different techniques. Each technique has its advantages and disadvantages. To choose the most appropriate technique, short descriptions are provided in this chapter and compared with the requirements of the system.

The variable delay line will need to be able to achieve a maximum delay of 10 µs. The signal should still be of excellent quality after being delayed as this will allow more efficient modulation codes. This means the SNR should be negligible attenuated and the wavelength

Time-delay range	order of 10 µs
Bandwidth	40x100 GHz
Accuracy	enough to prevent lock-out
Distortion	minimal
Reconfiguration time	$< \tau_c$

Table 4-1: Requirements of the VPDL for the proposed site diversity system.

dispersion should be limited as much as possible to preserve the quality of the signal. A third requirement is that the variable delay technique can support a wide bandwidth as a $1\,\mathrm{Tbit\,s^{-1}}$ data rate is pursued. To achieve this a collection of 40 International Telecommunication Union (ITU) DWDM channels with 100 GHz spacing is desirable. Another requirement is the accuracy or resolution of the delay. This is needed to synchronise the two signals from the different OGSs at the satellite. If the accuracy of the synchronisation is not high enough and therefore the symbol timing will overlap the DVB-S2 receiver will lock out.

The different characteristics of the VPDL will play different roles in the system. The time-delay range will act as an upper bound on the controller. If the to be compensated time difference is larger than the maximum achievable time-delay of the chosen VPDL it will be impossible to get within the allowed bounds of the receiver to lock to the signal as described in section 2-3. The same is true for the lack of accuracy of the VPDL as the steps are too big to get within the bounds of the receiver. The distortions caused by the VPDL will act as noise on the system, which will make it harder for the receiver to lock to the signal. The reconfiguration time adds a delay to the feedback of the system.

Different techniques for VPDL are discussed in the remainder of this chapter, with a conclusion in section 4-7. In the conclusion a selection will be made of possible VPDLs to use in the proposed system.

4-1 Switching photonic delay line

The most trivial switching delay line, also called programmable delay line, uses a binary structure. A binary photonic delay line uses a variation of lengths of fixed SMF delay line loops and the same number of 2x2 optical switches [31]. The switches can redirect the signal through a delay loop or skip the delay loop. By selecting some of the delay line loops the desired delay can be achieved. A 8-bit binary delay line exists of a delay line of length τ, a delay line of length 2τ, 4τ and so on till 128τ. Therefore a maximum delay of 256τ can be achieved with a resolution of τ. The great advantage of using simple SMF for the delay is that the it provides a true time delay. A true time delay is defined as an property of a transmitting apparatus and refers to invariant delay to wavelength of the signal. Thereby the method can achieve a long time-delay range as perturbations of the signal are limited. A disadvantage is that a switch accumulates noise [31]. This is partly crosstalk and partly insertion loss. To compensate for the losses a semiconductor optical amplifier (SOA) can be added to the system to amplify the signal [32]. The number of switches should still be limited. This can be done by using different switching structures as seen in Figure 4-1. The number of needed SOAs relative to the number of possible time-delay variations is represented as

$$y = k^{x/k}, \tag{4-1}$$

with y being the possible delay variations, k the number of selectable delay lines per switch and x the number of SOA. The optimal number of branches k per stage can be calculated to maximize the number of delays y. The optimum is at $k = 2.71$, but as the number of branches should be an integer the number of branches will be chosen as $k = 3$. When eight 3x3 switches are used it will be possible to vary the length with $3^8 = 6561$ stages instead of the $2^8 = 256$ stages when eight 2x2 stages are used. Increasing the switches to 4x4, while

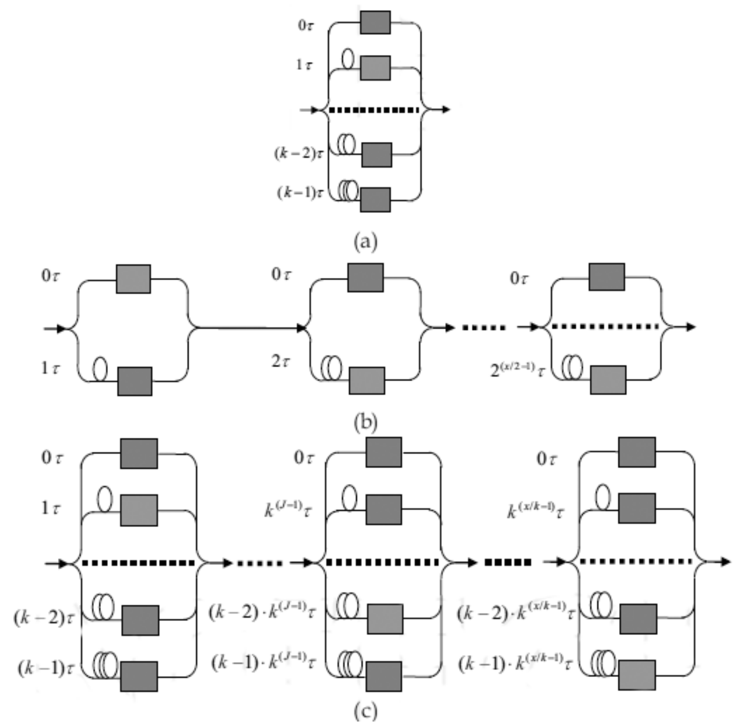

Figure 4-1: Three different types of programmable delay structure are shown. The boxes represent a SOA. In figure (a) the number of SOAs equals the amount of possible delays $y = x$. In figure (b) 2x2 optical switches are used resulting in $y = 2^{x/2}$. In figure (c) the possible delays are $y = k^{x/k}$, with k the number of branches [32].

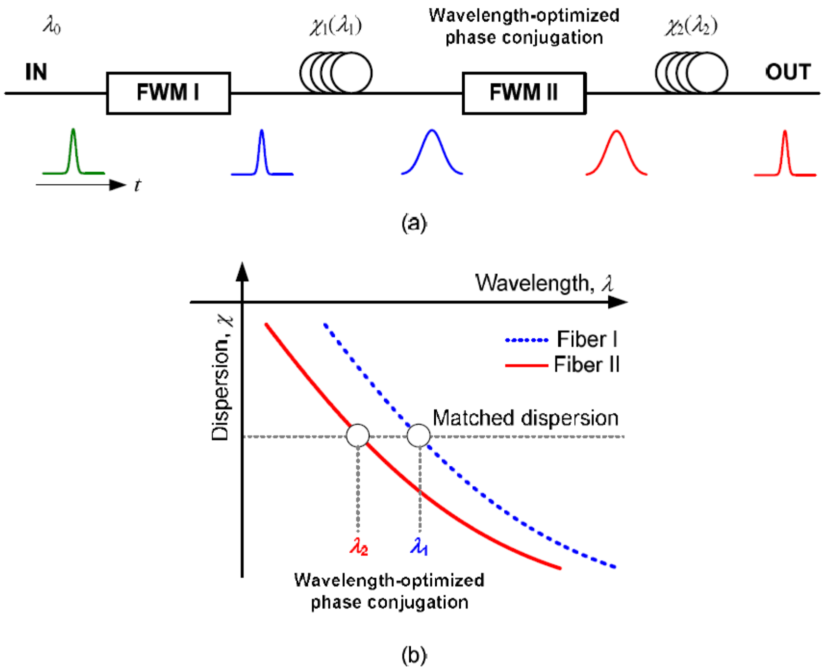

Figure 4-2: In figure (a) the delay generator based on two wavelength conversions and two dispersion fibers is depicted. In figure (b) the used principle for the compensation of the dispersion is shown. [36].

keeping the stages at 8, will further increase the number of possible delays but will decrease the ratio to needed SOAs as described in equation (4-1).

Even as the losses are partly compensated and the structure is optimised the time-delay resolution is limited due to the discrete number of SMFs. The lack of continuous variability can withhold the two signals from synchronising. Therefore it might be necessary to look at different VPDLs.

An optical switch influences the SNR level of the signal to a certain degree. Another important characteristic of a switch is the time it takes to switch. There are different kind of optical switches with varying performances. Examples of switching techniques are, MEM switches, silicon switches [33] and liquid crystals [34]. The signal losses as a result of the switches can partly be compensated by amplification methods like a Raman optical amplification [35]. However the performance of the switches it will always influence the quality of the signal and a trade-off will have to be made with the required switching time.

4-2 Wavelength conversion-based delay line

Another technique to control time-delay is to combine wavelength converters with high-dispersion fiber (HDF). HDF is made of a material which naturally disperse the group velocity of optical waves for different wavelengths. The propagation speed of the signal is thus depending on the wavelength of the signal. By converting the wavelength the time travelled and thus the time-delay induced by the HDF can be controlled. The time-delay as a result of dispersive fiber is expressed in the following equation [37].

$$\tau = DL\Delta\lambda, \tag{4-2}$$

with τ being the time-delay, L the length of the HDF, $\Delta\lambda$ the wavelength difference and D the group velocity dispersion (GVD) coefficient. The GVD coefficient is expressed as in ps/nm/km stating the induced time delay per wavelength difference per fiber length. After the signal is delayed the signal will be restored to the original wavelength by another wavelength converter. In a research by Dai in 2009 [36], as shown in Figure 4-2, a fourth stage is added where the signal is delivered into another HDF to compensate for the signal pulse broadening as a result of the first HDF. The broadening is a direct effect of the the dispersion as the signal consist of a variety of wavelengths.

The wavelength conversion can be done with different methods. The used method will also determine the resolution of the delay line. Most devices use a tunable laser source combined with four wave mixing to convert the wavelength. The tuning range and precision of the laser is then one of the defining factors for the delay line. The wavelength conversion adds noise and thereby degrades the original signal. Besides the wavelength tuning range the maximum delay can be increased by lengthening the HDF, but this is also limited as discussed in [38]. The loss and broadening of the signal caused by the high dispersive material can not endlessly be compensated and therefore will decrease the SNR. Thus to increase the maximum time-delay it will be necessary to extend the system with another technique to achieve continuous tuning and a large delay range. Another disadvantage of this technique is the base time-delay that will be added to the signal. This is the time needed for the signal to propagate through the material without considering the dispersion for the tunable time-delay.

4-3 Agile lens-based broadband variable delay line

In a study of N.A. Riza in 2010 a agile lens-based broadband variable delay line is discussed[39]. The optical signal enters the variable delay line through a fiber lens. At the self-imaging distance $2d_1$ [40] an electronically controlled variable focus lens (ECVFL) is placed. The ECVFL is used to focus the optical beam at a movable mirror positioned at d_2, as can be seen in Figure 4-3. By placing the mirror at the focal length it is ensured that the light travels the exact same path back to the ECVFL, thereby reducing unnecessary SMF-free-space coupling losses. The position of the mirror is controlled electronically and the settling-time depending on the used actuator will be in the order of ms [39]. Moving the mirror and the focal length of the ECVFL alters the travelled distance of the optical signal, hence the time delay. The position of the mirror determines the delay as described in the following equation:

$$\Delta T = \frac{2D_1}{v_{air}} \tag{4-3}$$

With D_1 the position of the mirror from the focus lens and v_{air} the speed of light in air. The dynamic range of the the variable delay line is conducted from the Gaussian beam propagation analysis. The path length difference range R of the VPDL is therefore defined by

$$R = d_{2\text{Max}} - d_{2\text{Min}}, \tag{4-4}$$

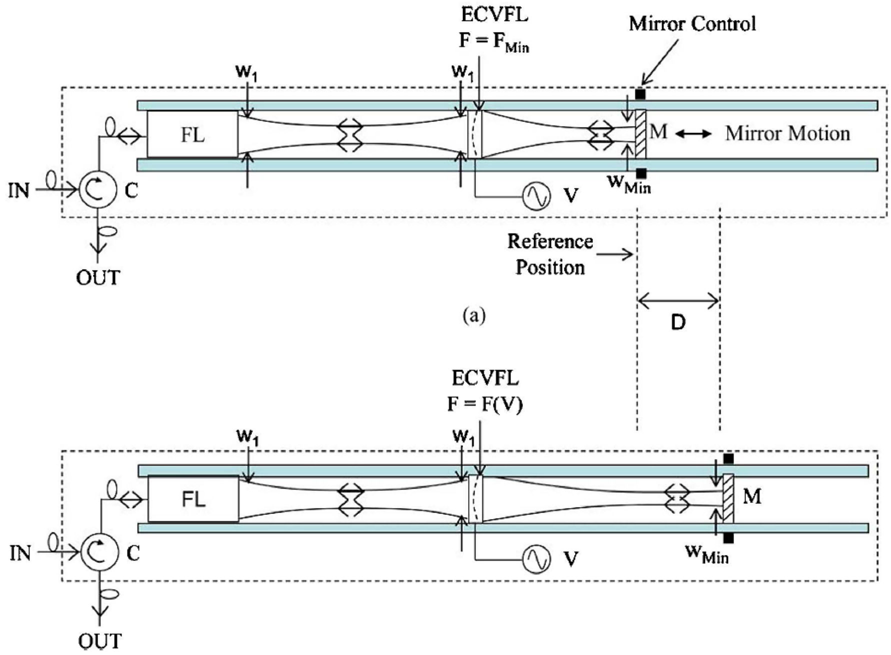

Figure 4-3: Agile lens-based broadband variable delay line proposed by N.A. Riza in 2010, [39].

with $d_{2\mathrm{Max}}$ and $d_{2\mathrm{Min}}$ the maximal and minimal focal lengths of the ECVFL. Resulting in a time-delay dynamic rang of

$$R_T = \frac{2(d_{2\mathrm{Max}} - d_{2\mathrm{Min}})}{v_{air}}. \tag{4-5}$$

The length difference range of the experimental setup is 15 cm [39]. The time-delay range is therefore 1 ns. The total expected losses of the system are 2.1 dB which is assumed very low for a VPDL with such a large range. This attenuation could even be improved to <1 dB by replacing the ECVFL and mirror by using a single broadband mirror-based ECVFL. The dimensions of the system built for the experiment in 2010 is a tube of 25 cm with a width of 1 cm. The setup could be scaled up to a time-delay of a few ns.

The agile lens-based VPDL is an technique which offers a few ns true time-delay range and a near continuous precision. Another advantage of this VPDL is the low loss of <1 dB. A disadvantage is the large settling-time to alter the position of the mirror, which can go up to a few seconds if the setup is scaled up [39].

4-4 Dynamic Brillouin grating-based delay line

The moving mirror is clearly not a desirable solution as the mechanical part will be subject to wear and the tuning speed is slow. Another solution which is based on the same principle of varying the path length of the signal by moving a reflector to a given position, is the use of a dynamic Brillouin grating (DBG) [42]. The signal is reflected at the generated grating for a given frequency. The DBG is generated in a highly birefringence material. Birefringence is the property of variable refraction index based on the polarization and the propagation

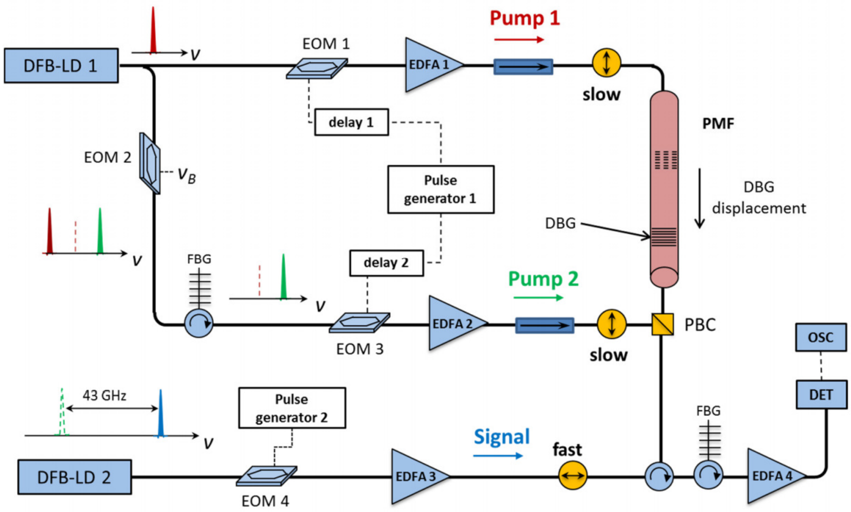

Figure 4-4: Representation of a dynamic Brillouin grating delay line. [41].

direction of the light wave. The fiber has a slow and a fast axis and the light transmitted in a certain polarizations maintains the polarization during propagation. By pumping two signals with the same polarization in opposite directions into the fiber a DBG is created as seen in Figure 4-4. The central frequency of the DBG is calculated using the following equation [37].

$$\nu_B = \nu_{P1} - \nu_{P2} = \nu_S - \nu_R, \tag{4-6}$$

with ν_{P1} and ν_{P2} the frequencies of pump 1 and 2. ν_S the frequency of the signal and ν_R being the frequency of the reflected signal. This is a result of stimulated Brillouin scattering which is an effect under phase matching conditions of the pump signals and is given by [41]:

$$\nu_B = \frac{2V_a}{c} N_x \nu_{P1}^x = \frac{2V_a}{c} N_y \nu_{P1}^y \tag{4-7}$$

n_x and n_y are the refraction indexes of the slow and the fast axis and V_a is the acoustic velocity in the fiber. The acoustic lifetime of the DBG in a normal fiber is around 11 ns. Therefore it is no problem to use this technique for delaying single pulses or short packets but delaying continuous data streams is not trivial. To enable the use of DBG delays for data streams the pumps will have to be repeated before the DBG is decayed. By repeating the pump pulses a quasi-permanent DBG will be created and therefore allowing continuous delays. As a result the maximum time-delay possible for continuous data streams is 11 ns as the repeating pump pulses will otherwise interfere on other locations in the fiber than the planned DBG location. The transit time of the signal must be less than half the repetition rate of the pumps [37]. The bandwidth of the reflected signal is inversely proportional to the spatial length of the grating. By using shorter pump pulses the bandwidth can be increased, but this will also decrease the reflectivity. This can be partly compensated by increasing the pump power. An advantage of the technique is that the broadening of the signal is not depended on the delay. A DBG should theoretically be able to delay a 10 Gbit s^{-1} data stream by 10 ns. This technique will have to be further researched before it can be applied in the existing communication techniques.

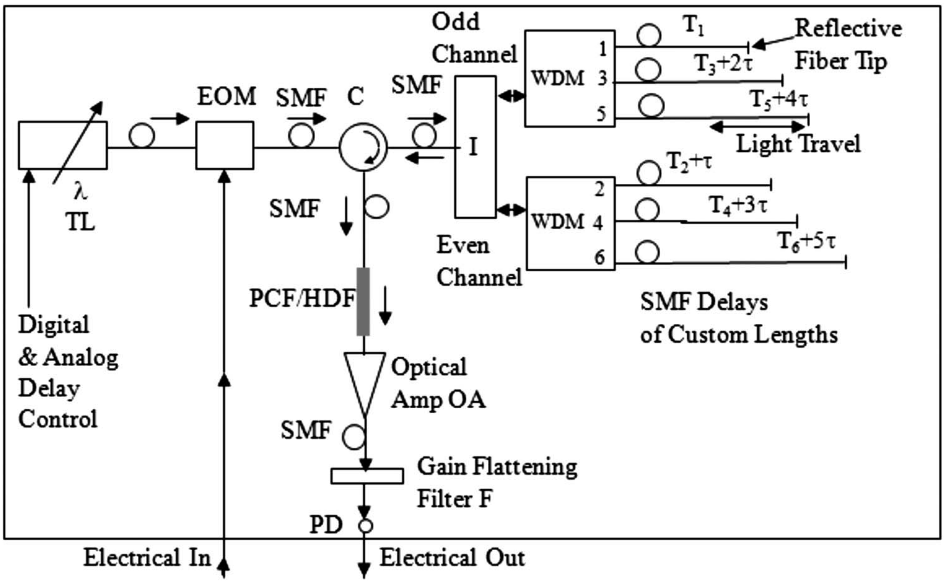

Figure 4-5: The switchless hybrid analogue-digital variable delay line as proposed by N.A. Riza. The variable delay line uses a tunable laser (TL), an interleaver (I), two WDM devices, variety of SMF lengths and a high-dispersion fiber (HDF) [40].

4-5 Hybrid analogue-digital

To solve the lack of continuous variability of a switching delay line the digital delay can be extended by an analogue tunable time delay. In a research from N.A. Riza [43] a wavelength convertor-based optical delay line is used to achieve an analogue delay up to 800 ps. By using switches extra delay lengths are added to achieve a maximum time delay of 25.6 ns. N.A. Riza also proposed a switchless hybrid analogue-digital delay line, thereby eliminating the time needed to switch to achieve a fast VPDL. The analogue delay is based on wavelength conversion and uses a HDF to tune the time-delay. The digital part exists of short SMFs to add discrete steps to the time-delay.

The DWDM signal enters the VPDL and is converted up or down using a tunable laser. The signal is then split into even and odd channels to reduce crosstalk as it doubles the channel spacing. Connected to the channels are a variety of lengths of SMFs as can be seen in Figure 4-5. The signal is then lead back to a HDF which will result in a delay depending on the wavelength. In the performed experiment a HDF with a dispersion of D =600 ps/nm/km is used. This will allow a tuning range with a channel wavelength spacing of $\Delta\lambda$ =1 nm to disperse τ =600 ps when a HDF of 1 km is used as defined by $\tau = DL\lambda$. A quick look at more recent studies show that photonic crystal fibers with a dispersion of more than 22 200 ps/nm/km at 1550 nm exist [44]. But the use of higher dispersive material is limited due to performance at high data rates [38]. The central wavelengths of the channels are defined as $\lambda_1, \lambda_2, \lambda_3 \ldots$ The SMFs attached to the WDM devices compensate for the channel specific bias that is a result of the dispersion for the central wavelengths of the channels. The added delays for the channels will be set as follows: $T_1, T_2 + \tau, T_3 + 2\tau \ldots$ The time-delay range will therefore be continuously tunable over a large range.

The performed experiment uses 16 channels to allow a time-delay range of 9.6 ns. The performance of a similar system proposed by Yitang Dai in 2010 achieves a time-delay range of 7.34 µs at a data rate of 10 Gbit s^{-1}, causing a penalty of 3.7 to 4.3 dB to the signal [38]. The performance of the time-delay range of this system is sufficient for the proposed system. More recent experiments show a 10 ns time-delay for a Gbit s^{-1} throughput [45].As this type of delay line has a limited data throughput it will be necessary to use multiple devices for delaying all the DWDM channels in the proposed optical feederlink to reach the 1 Tbit s^{-1} throughput.

4-6 Delay lines with limited performance

Phase shifters can be used to delay a microwave photonic signal. By changing the phase the signal is delayed. The maximum delay that theoretically can be achieved is one period of the signal. Due to this limitation it will be impossible to use this technique for the application of synchronising OGSs. The wavelength of the signal in L-band is around 15 to 30 cm and the necessary path length correction can exceed multiple kilometre.

Variable delays for radio frequencies (RF) signals can also be achieved by the use of ring resonators[46]. The main disadvantage it that a ring resonator is only applicable for a limited bandwidth and a limited delay. To achieve a wide bandwidth it will be necessary to use numerous ring resonators which will be difficult to control. As the goal of this thesis to achieve an optical feederlink with a throughput of 1 Tbit s^{-1} the delay line should support a bandwidth of approximately 40x100 GHz. Therefore this option is discarded as the system will be too complex.

Another existing variable delay line is a slow-light delay line. The principle uses stimulated Brillouin scattering to temporary adjust the density of the medium and thereby decreasing the speed of the signal due to a Doppler effect. This technique however is limited in bandwidth and can only delay the signal for a few bits [47].

4-7 Conclusion

All the delay line techniques discussed in this chapter still need to be further developed, before they can be implemented in the proposed site diversity system. The only commercially ready option for a high throughput signal is the switching technique, but the limited fine tuning will be a problem in the synchronisation of the OGSs.

Therefore it will be necessary to combine different techniques to achieve a VPDL with a large time-delay range and a fine tuning. Wavelength dependent techniques are previously combined with discrete switching techniques as in [40, 38]. But the use of HDF limits the bandwidth of the signal. It will only be possible to delay one DWDM channel with the proposed devices and thus a total of 40 devices will be needed. Agile lens-based broadband variable delay line has no broadband limitations as it provides a true time-delay. A disadvantage of this technique is the moving mirror which will be subject to wear. Also the adjustment speed of the mirror will an important factor as the atmosphere can change every 2 ms as discussed in section 2-5. The DBG-based technique has great potential as a variable delay line, but further research is required to investigate the possibilities.

Bidirectional use of the proposed techniques will also have to be further investigated. As in the ideal situation, as the proposed system in section 3-4, the uplink will use the exact same path as the training sequence from the beacon signal coming down. The programmable delay lines are bidirectional as they make solely use of switches and SMF which have no directional limitations. The other techniques will have to be adapted to be implemented in the proposed system.

At the moment only the programmable delay line is ready to be implemented in the system. Therefore we will assume to use this technique in the simulations. Part of the simulations will be to investigate what precision will be needed from the VPDLs. We can then conclude if the digital approach of a programmable time delay will be sufficient.

	Switching	WC-based	Lens-based	DBG-based	Hybrid
Time-delay range	trade-off with accuracy	<10 ns	<10 ns	<10 ns	<10 µs
Bandwidth	40x100 GHz	∼100 GHz	40x100 GHz	∼100 GHz	depending on analogue part
Accuracy	trade-off with time-delay range	accurate	accurate	accurate	accurate
Distortion	low, depending on # of switches	larger time delay is more broadening	low	broadening factor independent of delay, reduced by increased pump power	depending on analogue part
Reconfiguration time	∼1 ms	>5 µs (desired time delay + optical length of dispersive medium (∼1 km fiber))	>100 ms	≈desired delay time	coarse tuning ∼1 ms, fine tuning dependent on analogue part

Table 4-2: Comparison of the VPDL performances.

Chapter 5

Control strategy

The objective is to compensate the difference in time delay of the uplinks via the two optical ground stations (OGSs). The controller should compensate for the fixed time delay difference and the disturbances acting on the system. The disturbances acting on the system are the movement of the satellite and the atmospheric turbulences. These disturbances are unknown. The objective of the controller is thus to equalise the travelling times, Δt_1 and Δt_2, of the signals by adding a time delay t_a.

To show the influence of t_a on the system and Δt_1 we assume the situation without satellite movement and without atmospheric turbulences. The system consists of the terrestrial fiber and the atmospheric channel. Without the added time delay t_a of the variable photonic delay line (VPDL) the minimal time delay of the received signal $\Delta t_{1,\text{min}}$ is achieved at the output. The difference of $\Delta t_2 - \Delta t_{1,\text{min}}$ will have to be compensated by t_a to result in $\epsilon = 0$ as

$$\epsilon = \Delta t_2 - (\Delta t_{1,\text{min}} + t_a). \tag{5-1}$$

5-1 Feedback delay

A conventional method would be to measure the performance of the system and use the output to deduce the disturbances. The deduced knowledge about the disturbances could then be used to compensate the time delays and improve the performance of the system. This method is called a feedback system as the performance of the output is fed back to the controller. A disadvantage of this method is the lag between the output measurement and the controller. The feedback compensation is always lagging behind by definition. Especially in this system where the feedback delay is very large compared to the rapid change in disturbances. The feedback delay consist of the travelling time from the control centre to the satellite where the performance is measured. From there the feedback will be sent back down to the control centre. Therefore the feedback delay is at least 250 ms and the system might be too late to react to sudden changes of the satellite position and atmospheric changes. We could therefore state that the feedback delay should be reduced to a minimum.

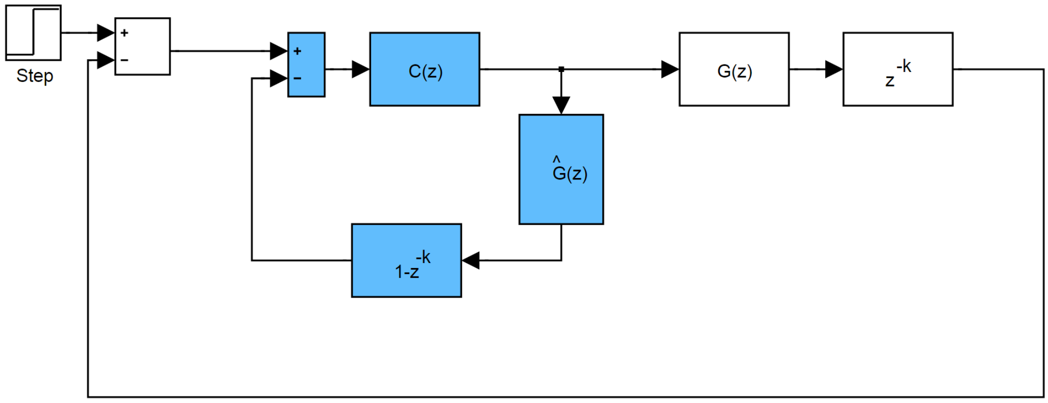

Figure 5-1: System diagram of Smith predictor.

5-2 Feedforward control

Feedforward control is a method which is not based on a feedback loop, but compensates for the disturbances without direct measurements of the performance output. Feedforward control is a preferred option as feedback control is late by definition. The problem with feedforward control is the lack of knowledge about the disturbances.

With feedforward control we will not directly measure ϵ, which would imply measuring systems on the satellite. The feedback lag introduced by the distance from the OGSs towards the satellite is reduced as the information about the satellite movement will reach the controller within 125 ms. This is an improvement of 125 ms compared to the use of standard feedback delay. In the situation without disturbances the measurement equals the ideally measured output $\hat{\epsilon} = \epsilon$. If $\Delta t_{1,\min} + t_a > \Delta t_2$, t_a will have to be reduced. In the other case t_a will be increased to get the desired value of the control value t_a as

$$t_a = \Delta t_2 - \Delta t_{1,\min}. \tag{5-2}$$

In the real world the satellite movement will constantly change the difference between Δt_2 and $\Delta t_{1,\min}$ and a discrepancy of the measurements $\hat{\epsilon}$ and ϵ will arise. The atmospheric turbulences will also add noise to the measurements and the received signal. The noise added to the measurement and the system will have a certain correlation, due to crossing the same atmospheric channel in opposite directions. For a static 7 km distance a signal correlation was measured of 0.993 [29]. The correlation that applies to the proposed system will have to be further investigated.

The measurement of $\hat{\epsilon}$, which is the travelling time difference of the two downlink signals, will be done by cross correlation on the downlink sequences. This measurement can then be used to control the VPDL to achieve $\hat{\epsilon}$ to be minimum following this equation.

$$\hat{\epsilon} = \Delta t_{2d} - (\Delta t_{1d,\min} + t_a) \tag{5-3}$$

5-2-1 Smith predictor

The proposed parallel system in section 3-4 used to estimate the influence of the disturbances on the system has similarities with a Smith predictor [48]. A Smith predictor is designed to

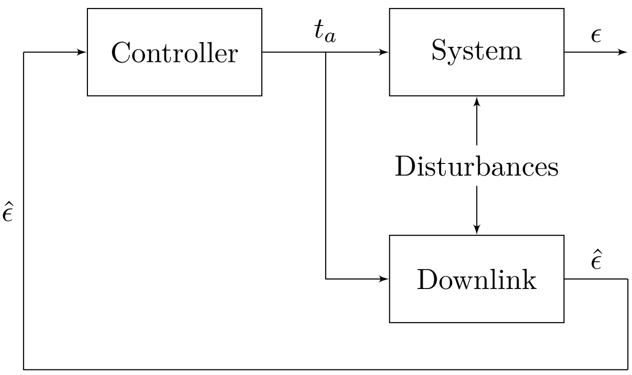

Figure 5-2: Block diagram of the proposed system. The block named downlink is the added parallel system to acquire knowledge about the disturbances acting on the system.

cope with a time delay in the system.

To apply a Smith predictor on a plant $G(z)$ with a time delay z^{-k}.To start, we consider $G(z)$ without a delay and design the controller $C(z)$. The closed-loop transfer function is defined by

$$H(z) = \frac{C(z)G(z)}{1 + C(z)G(z)}. \tag{5-4}$$

The next step is to design a controller $\bar{C}(z)$ for the time delayed plant $G(z)z^{-k}$, with the goal that the closed loop transfer function $\bar{H}(z)$ should equal $H(z)z^{-k}$. Solving the following equation

$$\frac{\bar{C}Gz^{-k}}{1 + \bar{C}Gz^{-k}} = z^{-k}\frac{CG}{1 + CG}, \tag{5-5}$$

will result in:

$$\bar{C} = \frac{C}{1 + CG(1 - z^{-k})}. \tag{5-6}$$

The Smith predictor uses a model of the real system to calculate the optimal controller. Disturbances are corrected by a second loop as shown in Figure 5-1. This feedback loop contains the undesired lag, but corrects the accumulating effects of disturbances in the long run.

The considered time delay compensator has no specific dynamics and the controller should be focussed on compensating the disturbances on the system. As the Smith predictor can not provide a disturbance compensation without the lag induced by the system, the performance will not suffice for our system.

5-2-2 Proposed controller

The proposed system in section 3-4 uses a parallel system to gain knowledge about the disturbances. The parallel system is a downlink signal transmitted by the satellite towards both OGSs. The downlink signal travels using the same path as the uplink signal, thereby being influenced by the same disturbances. The disturbances are a combination of satellite movement and atmospheric turbulences. The knowledge of the disturbances deduced by the measurements on the downlink signals can be used to feedforward control the uplink signals.

The controlled system is shown in Figure 5-4. The performance metric is the timing difference, ϵ, which should be minimised, as a high timing difference will increase the chance of receiving erroneous packets. Due to the several error correction methods present in the Digital Video Broadcasting - Satellite 2nd generation (DVB-S2) standard, it is difficult to state an allowed threshold for ϵ. Measuring ϵ and using the value to control the system would induce a great feedback delay. The lag in the system will cause problems as the measured performance only contains information about the control performed at least 250 ms before. By adding a parallel system to measure the disturbances directly the lag is shortened by 125 ms, as the timing difference will be measured at the control centre. The information of the travelling time can then be used to apply feedforward control. The measurement of the timing difference $\hat{\epsilon}$ is thus an estimation of the performance metric ϵ.

The chosen variable delay line technique will have no dynamics. As it consist of a concatenation of switches and delay lines as is described in section 4-1. The controller will therefore only need the right setpoint, which will be based on the measurements done on the downlink. The measurement system uses correlation to determine the timing difference of the two downlink signals. It will be important that the setpoint does not make abrupt changes due to individual erroneous outputs of the measurement system. An integrator will therefore be ideal as this will always stabilise the system towards the setpoint.

5-3 Disturbances

The disturbances acting on the system are an important part of the controller design. The main disturbances acting on the performance metric are the satellite movement and atmospheric turbulences. The satellite movement will behave smoothly and most of the time can be estimated using complex calculations. The position of the satellite is corrected by specific manoeuvres whenever the satellite is disturbed out of the specified orbit. The atmospheric turbulences will add noise to the travelling time of the links. These disturbances will have less of an impact on the timing difference but are far more difficult to estimate. This is a result of the nature of the disturbance as the atmosphere is a very complex system.

It will be important that the controller closely follows the satellite movement without acting constantly on the noise as a result of the atmospheric turbulences. This excludes the use of the derivative part of a proportional-integral-derivative (PID)-controller. The atmospheric turbulences might heavily influence the controller while the satellite movement behaves differently. As the concatenated switches do not have any dynamics to cope with, the proportional part is not necessary and only an integrator will be used. This results in a stable controller with a minimum steady state error.

5-3-1 Quantisation error

The use of cascading switches will result in a quantisation error as the accuracy of the timing compensation will be limited. This is dependent on the length and the number of delay lines used to compensate for the time-delays. The precision of the VPDL limits the performance of the controller.

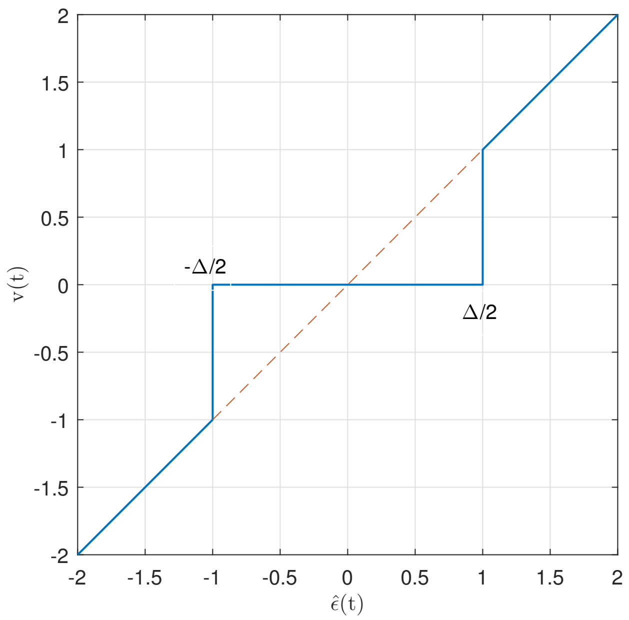

Figure 5-3: Representation of the adapted deadzone used in the controller.

The discrete character of the VPDL in combination with the integrator controller results in an unstable system as the accumulating quantisation error will always result in a delay line switch. Even if the selected delay line length is already optimal for the measured timing difference. For instance when the precision of the delay line compensator is set at 10 steps and the measured delay difference is 751 steps. The controller is therefore set at 750, but every iteration the integrator will add a value of 1 as the added delay is off by 1 step. After 10 iterations the integrator will set the controller at 760, while this is not the optimal setting for the given situation. This example is shown in the top graph of Figure 5-5.

To solve this problem a deadzone is introduced. A deadzone is a region of the inputs which results in an output of zero. The deadzone is half the length of the shortest delay line and will prohibit the measured timing difference error to contribute to the controller. For instance, if the shortest delay line is 1 ns and the measured timing difference is less than 0.5 ns the measurement will not contribute to the controller. Therefore no change in the time delay compensator will be made. A deadzone normally decreases the output by the deadzone limits. We adapt this by adding an offset depending on the sign of the input, thereby compensating the decrease of the output. The resulting function is shown in Figure 5-3. The effect of adding the adapted deadzone to the controller can be seen in Figure 5-5 The first figure is without a deadzone and the second is with the adapted deadzone implemented.

5-4 Mathematical representation

For implementation the controller is described using mathematical equations. The controller exists of an integrator combined with an added deadzone. The integrator uses the forward Euler method. Afterwards quantisation is done by the concatenated delay line switches.

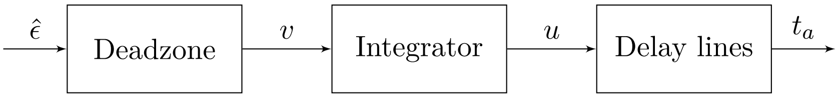

Figure 5-4: Block diagram of the controller. $\hat{\epsilon}$ is the measured timing difference of the downlink sequence. t_a is the added time delay.

Mathematically this can be expressed using the following equations:

$$u(n) = u(n-1) + I \cdot T_s \cdot v(n-1) \tag{5-7}$$

with I the integrator gain, T_s the sample time and

$$\tag{5-8}$$

$$v(n) = \hat{\epsilon} \qquad \text{if } |\hat{\epsilon}(z)| > \frac{\Delta}{2} \tag{5-9}$$

$$v(n) = 0 \qquad \text{if } |\hat{\epsilon}(n)| \leq \frac{\Delta}{2} \tag{5-10}$$

Where $\hat{\epsilon}$ is the measured timing difference of the downlink sequence and Δ is the precision of the time delay compensator. Δ is the delay time precision that corresponds to the shortest delay line length. The output $u(n)$ has a lower limit of 0, as a negative time delay will be impossible to implement. A upper limit can be set corresponding to the largest possible added time delay of the system. The result $u(n)$ is then led into the structure of concatenated delay lines which quantises the resulting added time delay t_a.

$$t_a(u) = \Delta \cdot \text{round}\left(\frac{u(n)}{\Delta}\right) \tag{5-11}$$

The resulting t_a will alter the timing difference of the uplink and therefore the performance of the system. At the same time t_a alters the timing difference of the downlink sequence and thereby changing the measured output $\hat{\epsilon}$, which results in a new setpoint for the controller.

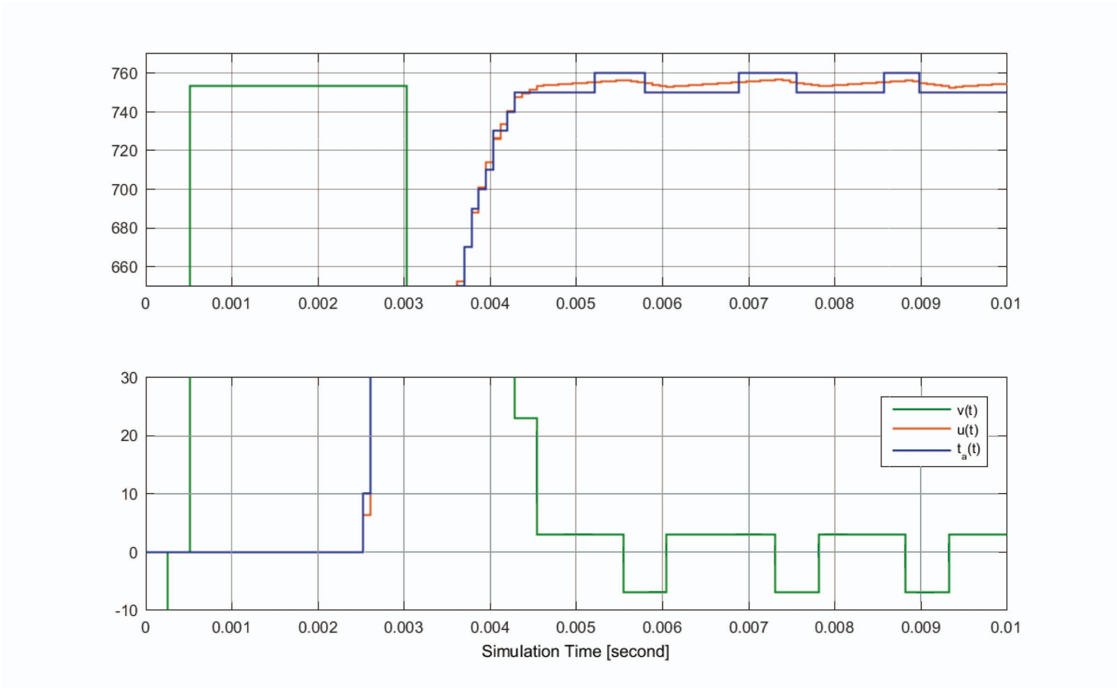

(a) Behaviour of the controller without implementation of a deadzone. The added delay line keeps changing, while the optimal setting has already been reached.

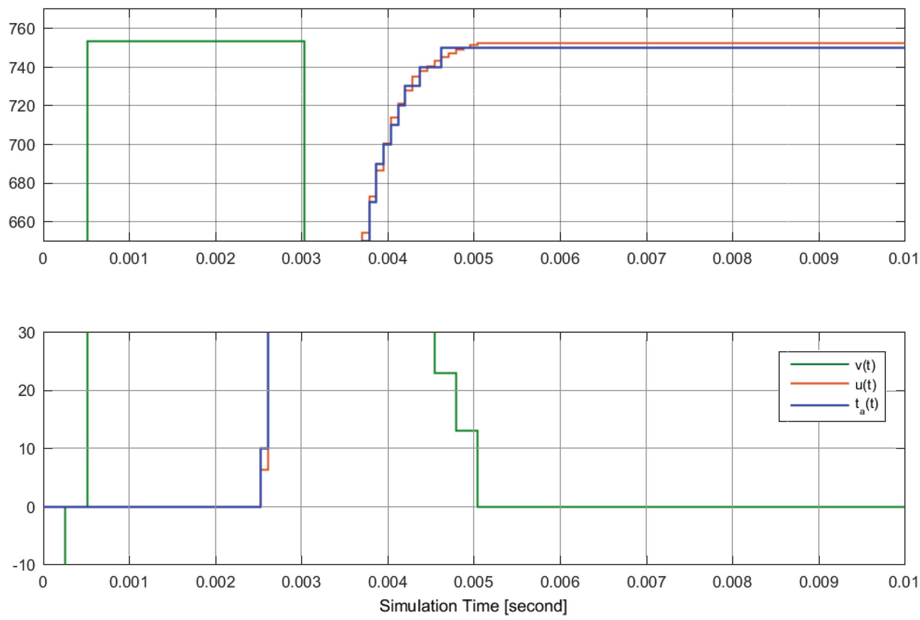

(b) Behaviour of the controller with implementation of a deadzone. When the timing difference gets within 5 steps of 0 the value of v(t) is 0 resulting in a stable compensator.

Figure 5-5: Comparison behaviour of the controller without and with implementation of a deadzone. The green line represents the input of the integrator. The red line is the output of the integrator and the blue line is the added time delay.

Chapter 6

Simulation model

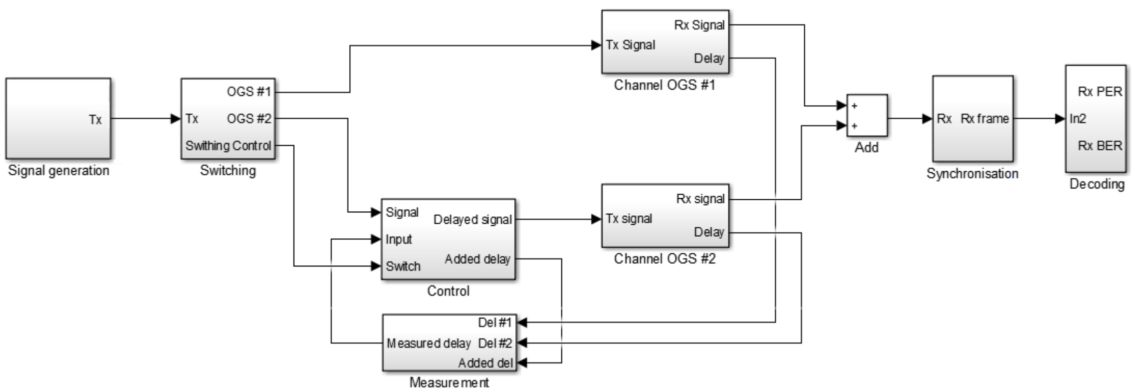

Figure 6-1: Overview of the simulation model containing the different subsystems.

The model used for simulating and monitoring the performance during a switch between optical ground stations (OGSs) is built in *Simulink* [49]. The model contains the generation of the signal following the DVB-S2 standard [8], two transmission channels and a receiver part. The desired site diversity is modelled by the use of two different transmission channels. The objective of the simulations is to evaluate the performance of the system during a switch between the two transmission channels. The two channels represent the path of the signal from the control centre to the receiver using two different OGSs. The time delay difference between the two paths will be measured within the model and the measured output will be used to compensate the time delay of one of the two channels.

First the standard model of the transmitter and the receiver will be discussed. This model is based on two example models provided in the communication toolbox by Mathworks. The "DVB-S2" example [50] is used as a base for the signal encoding and some building blocks of the "QPSK Transmitter and Receiver" example [51] are used as a base for synchronising the receiver. Unless stated otherwise the simulated link uses the DVB-S2 standard and is modulated using quadrature phase shift keying (QPSK) with a forward error correction (FEC) rate of 1/2. This is a widely used modulation code and a conservative choice in current satellite links. The choice is made to rule out any performance issues due to the modulation code. The simulation model does not specifically apply to the use of an optical link, but uses a generic signal transmission and receiving process. This is due to the fact that the downlink is in radio frequencies (RF) and several other generic sources of distortions in the equipment are still present in the planned system. The diversity of the different distortions and disturbances will result in random noise. Therefore white noise and a variable delay is added to the transmission channels to simulate the distortions as a result of the different process parts as described in 6-2. Calculations are done per frame to speed up the simulation process. In section 6-6 and 6-7 the planned additional segments are discussed to enable seamless switching. These segments contain a measuring part and a controlling part. An overview of the simulation model is shown in Figure 6-1.

6-1 Signal generation

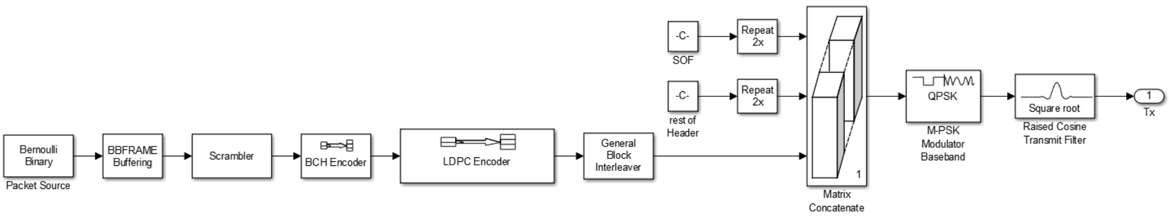

Figure 6-2: Overview of the DVB-S2 signal generation in the simulation model. SFRAMEs are not considered in this figure.

In this part of the model the data is generated and structured following the DVB-S2 standard. The transmitted data is represented by a random bit sequence generated by a Bernoulli bit generator. The bit rate is calculated from an assumed symbol rate of approximately 400 Msym/s, which translates roughly in a symbol time of 2.58 ns. 400 Msym/s is chosen as this symbol rate will be possible to achieve in the near future according to an expert from modem manufacturer Newtec [52]. The data is generated in frames of 1504 bits representing a MPEG packet. These frames are buffered and zero padded to achieve base-band frames (BBFRAMEs) of 32208 bits. The frame rate of the system is then $8.4 \times 10^{-5}\,\mathrm{s}^{-1}$.

6-1-1 Scrambler

After this the frames are scrambled. Scrambling is a technique used to prevent succession of multiple zeros or ones [49]. The scrambling polynomial used in the simulation is [1 1 1 0 1] and is reset at the beginning of each frame.

6-1-2 BCH encoder

The next step in the signal generation is the data being Bose and Ray-Chaudhuri (BCH) encoded [53]. This is done for error correction as described in section 2-3. BCH encoding can correct a specified number of errors. The decoding uses an algebraic method called syndrome decoding, which is easy to implement in an electrical circuit [53]. The output of the BCH encoder is the BBFRAME containing the codewords of 32400 bits. N is the length of the codeword and K is the length of the message. $N - K$ is the number of parity check digits being $32400 - 32208 = 192$. The added parity check digits contain information that can be used to correct errors in the received frames. The used BCH generator polynomial is $g_1(x) = 1 + x^2 + x^3 + x^5 + x^{16}$.

6-1-3 LDPC encoder

The BCH encoded frame is then low-density parity-check code (LDPC) encoded [54]. The simulation uses a FEC rate of 1/2. The transmitted information will be transmitted in twice the number of bits to be able to correct received errors. For this the LDPC uses a parity check matrix. The matrix consist of binary codewords of length n containing of information digits, k, and check digits, r. The size of the matrix is r by n. The codewords are modulus 2 equations which equal zero as shown in the example in equation 6-1 [55].

$$\begin{aligned} c_1 \oplus c_2 \oplus c_3 \oplus c_5 &= 0 \\ c_1 \oplus c_2 \oplus c_4 \oplus c_6 &= 0 \\ c_1 \oplus c_3 \oplus c_4 \oplus c_7 &= 0 \end{aligned} \tag{6-1}$$

The parity matrix, $H = [-P^T | I_{n-k}]$, representing these equations is then:

$$\begin{bmatrix} 1 & 1 & 1 & 0 & 1 & 0 & 0 \\ 1 & 1 & 0 & 1 & 0 & 1 & 0 \\ 1 & 0 & 1 & 1 & 0 & 0 & 1 \end{bmatrix}$$

The matrix restricts the possible valid codewords. A four-bit message is now represented by a seven-bit message containing three redundant bits. The valid messages are generated using the generator matrix $G = [I_k | P]$. The result of $GH^T = 0$ as the matrices should be orthogonal.

6-1-4 Interleaver

The signal is lead into the interleaver, which rearranges the symbols in the frame. The reason for this is is to enhance the chance of recovering the frame in the case of signal loss. The impact of losing 10 consecutive symbols is more severe than 10 symbols spread over the frame. In the DVB-S2 standard column-wise interleaving is used by writing the data in rows and running through it vertically [9]. For QPSK signals the interleaving is not used as the chances of losing many bits is considerable lower than with 8PSK, 16APSK or 32APSK. In most simulations done for this thesis the interleaver is thus disabled.

6-1-5 PLFRAME header insertion

After the interleaving a header of 90 bits is added. The header consists of a start of frame (SOF) of 26 symbols and 64 symbols containing information about the following physical layer frame (PLFRAME). The SOF of a DVB-S2 signal is composed of the number $18D2E82_{\mathrm{HEX}}$ written in binary [9]. The SOF is later used by the receiver to synchronise the receiver to the frames. The following 64 symbols containing information about the modulation and coding (MODCOD) is chosen at random as the information is not vital in the simulation of the system.

6-1-6 SFRAME

In the case of the use of SFRAMEs, as described in 2-3-1, the PLFRAMEs are buffered in 6803 blocks of 90 symbols to the size of the information containing part of the SFRAME, which is 612270. A start of super frame (SOSF) of 270 symbols is composed of a 256 bit long Walsh-Hadamard sequence with 14 bits of padding. The 256 bits are one of the rows of the H_{256} matrix. The padding consist of the cropped H_{16} matrix, deleting the first and last column and repeating the matrix vertically. The resulting total matrix of 256x270 is the set of 256 possible SOSFs [9].

6-1-7 Modulation and raised cosine transmit filter

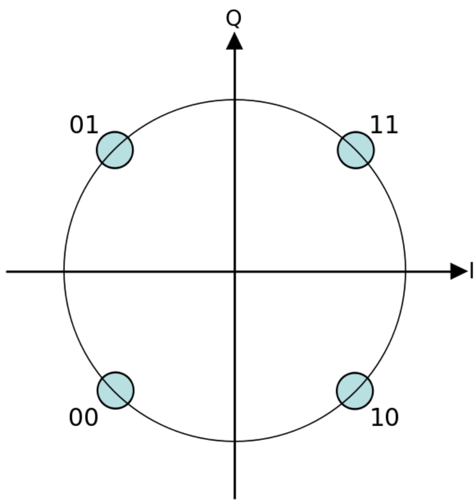

Figure 6-3: Constelation diagram of a QPSK modulated signal. Every symbol contains two bits.

The next block modulates the signal in a QPSK constellation. Thereby transmitting two bits per symbol. The constellation for QPSK is described in Figure 6-3.

6-1-8 Raised cosine transmitter filter

After modulation the signal is lead through a square-root raised cosine transmit filter to minimize the amount of inter symbol interference (ISI) [49]. This is done by pulse shaping the signal according to the rolloff factor. The filter in the simulation uses a rolloff factor of 0.5 and an upsampling rate of 4. The rolloff factor is the amount of excess bandwidth of the filter. The upsampling rate dictates the number of samples per symbol.

6-2 Transmission channels

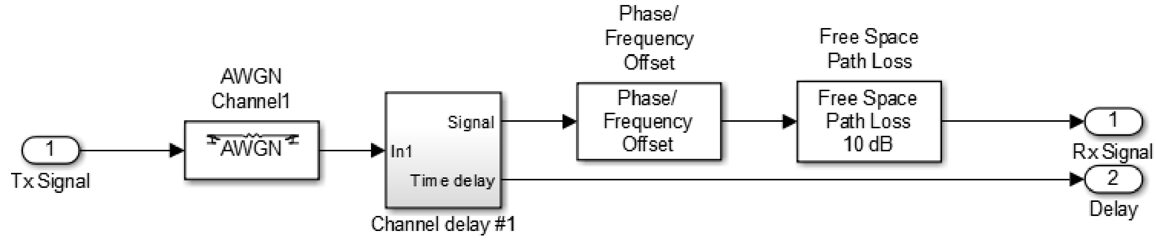

Figure 6-4: Block diagram of the transmission channel. First AWGN is added, then a variable time delay. The transmission also includes a phase and frequency offset and a free space path loss to reduce the gain. The added time delay output in the diagram is used to simulate the downlink time delay.

The transmission channel consists of some added distortions to simulate the effects of equipment and atmosphere as seen in Figure 6-4. To contribute for different arbitrary effect AWGN is added to the signal. Path loss is added to simulate the decrease in gain over the transmission channel. Phase and frequency offsets are added to simulate the behaviour of the modulator and the atmosphere. The simulation model contains two transmission channels to represent links via two OGSs. Switching in the simulation model occurs at the beginning of the channels by switching one channel off and simultaneously transmitting the signal through the other channel. The switching is controlled by the same signal which is timed to change at the beginning of each frame. At the end of the transmission channels both signals are added together to generate the received signal. As this would be the case on the satellite. Accurately timed switches on the satellite would be difficult. The added delays can cause the signals from the two OGSs to overlap for a short period of time during the switching process. The goal of adding the controlled compensation system is to prevent the overlap.

6-2-1 Time delay

To both transmission channels a time delay is applied. The added time delays are variable and intend to simulate the movement of the satellite. The maximum velocity of the satellite referenced to the OGS is assumed to be $4\,\mathrm{m\,s^{-1}}$ as this is the maximum velocity recorded referenced to the earth's surface in the dataset of satellite Astra 4B of the month May in 2016. This translates into an approximate time delay change of 13 ns per second. One step in the simulation is 646 ps. To simulate the maximum velocity of the satellite the time delay should change approximately 20 steps in 1 s. This is simulated using a sine wave with an amplitude of 20 steps and a frequency of $1\,\mathrm{rad\,s^{-1}}$. As the the locations of the two OGSs will be roughly the same referenced from the satellite the inflicted change in time delay difference between the two OGSs will be smaller. The data set provided by the SES flight dynamics team show a maximum change of $10\,\mathrm{cm\,s^{-1}}$. To simulate the maximum time delay difference the time delay of transmission channel #2 will be the sine function used in transmission channel #1 time shifted by 0.1 step as shown in Figure 6-5.

To simulate turbulences in the atmosphere AWGN is added to the applied time delays. The variance of the white noise is based on the 0.2 µs fluctuations of path length per metre mea-

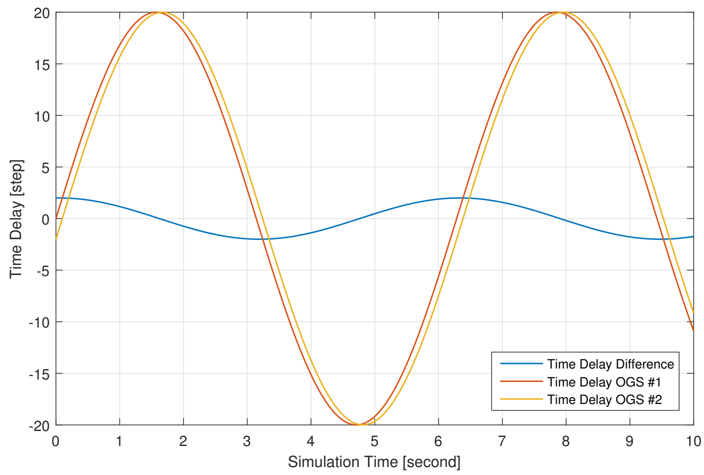

Figure 6-5: Simulation of the variation of the time delays as a result of the movement of the satellite. The orange and red lines correspond to the simulated variable time delay per OGS. The blue line is the resulting timing difference.

sured by Gibson [56]. This number is multiplied by 100 km to account for the length of the atmosphere.

The simulated time delays are designed to have the same delay fluctuation per second, but the amplitude of the sine wave does not correspond to the total fluctuation changes as in the the real world. This is done to investigate the behaviour of the system more thorough at a certain region. The total amount of time delay of the system is not simulated as the delaying the data by 250 ms has a huge impact on the memory usage. As this fixed delay is the same for both transmission channels there is no influence on the behaviour of the system. The simulated situation is thus of two OGSs for which the time delay is already compensated by a fixed delay line. Only the variable part of the time compensation is considered.

This of course also has an impact on the controller behaviour as the feedback lag is dramatically reduced. The impact of this reduced lag is not necessarily big. The timing difference will change at a maximum rate of $0.33\,\mathrm{ns\,s^{-1}}$. The reduced lag of 125 ms will therefore induce a maximal error of $\frac{1}{16}^{\text{th}}$ of the smallest control precision of 646 ps.

6-3 Synchronisation

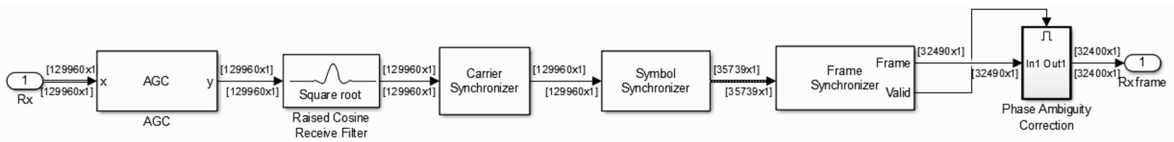

Figure 6-6: Overview of the synchronisation part of the receiver. The AGC is used to compensate gain differences, the carrier and symbol synchroniser is used to improve the acquiring time of the samples. The frame synchroniser and phase ambiguity corrector uses the known header symbols to align the symbols accordingly for the decoder.

The synchronisation part of the receiver adjusts the signal to improve acquisition and makes sure the samples are acquired from the received signal at the right moments. This process improves the received signal significantly as can be seen in Figure 6-8b.

6-3-1 AGC

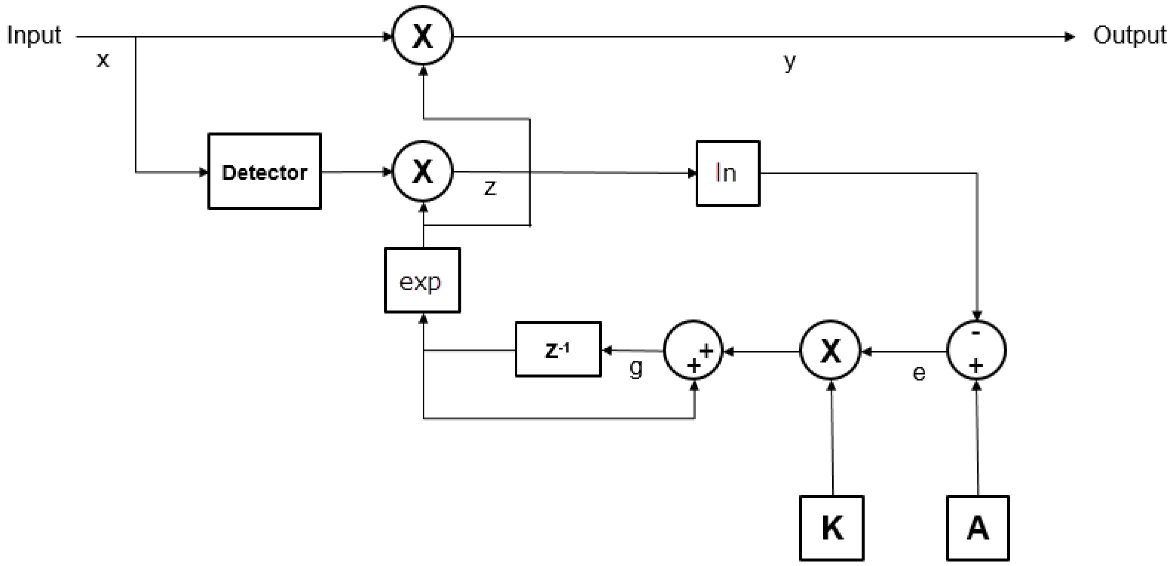

Figure 6-7: Diagram of the AGC, which is used to control the gain of the received signal. [49]

First the received signal is lead through the AGC which adjust the gain of the signal to be $1/\sqrt{4}$ as the samples per symbol is 4 and the total gain per symbol will then be equal to 1. To do this the AGC uses the logarithmic loop shown in Figure 6-7. The logarithmic loop of the AGC has an output signal which is the product of the input signal and the exponential of the loop gain [49]. The difference between the reference level and the product of the logarithm of the detector output and the exponential of the loop gain is defined as the error signal. The error signal is multiplied by the step size and passed through to an integrator.

The mathematical expressions to describe the behaviour of the loop are:

$$y(n) = x(n) \cdot \exp(g(n-1)) \tag{6-2}$$
$$z(n) = D(x(n)) \cdot \exp(2g(n-1)) \tag{6-3}$$
$$e(n) = A - \ln(z(n)) \tag{6-4}$$
$$g(n) = g(n-1) + K \cdot e(n), \tag{6-5}$$

where
x represents the input signal.
y represents the output signal.
g represents the loop gain.
$D(\cdot)$ represents the detector function.
z represents the detector output.
A represents the reference value.

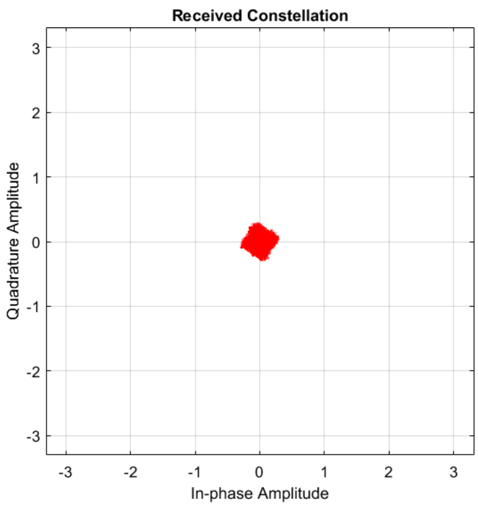

(a) The received samples before synchronisation. The samples are packed and contain a lot of noise. Different symbols are hard to recognise.

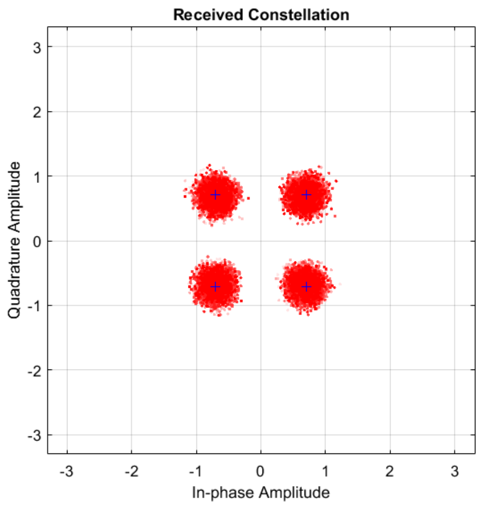

(b) The received samples after synchronisation. The symbols are easily recognised. The red dots represent the synchronised samples and the blue crosses show the supposed constellation.

Figure 6-8: Constellations of the received signal before (on the left) and after (on the right) synchronisation.

e represents the error signal.
K represents the step size.

The used detector is a square law detector, the output, z, is given by [49]:

$$z(m) = \frac{1}{N} \sum_{n=mN}^{(m+1)N-1} |y(n)|^2, \tag{6-6}$$

where N represents the update period of the detector.

6-3-2 Raised cosine receive filter

The gain adjusted signal will then be filtered by the raised cosine receive filter with a rolloff factor of 0.5. The upsampling 4 done by the raised cosine transmitter filter is remained. The samples are usefull in the following steps of the synchronisation of receiver.

6-3-3 Carrier synchroniser

Frequency offset is a result of three factors. The oscillator of the modulator and of the oscillator of the demodulator will have no influence on the switching of the channels as both channels will use the same modulator and demodulator. The third effect is the Doppler effect which is a shift in frequency due to the movement of the source or receiver. The frequency shift, Δf as a result of the Doppler effect is calculated using the following equation:

$$\Delta f = \frac{\Delta v}{c} f_0, \tag{6-7}$$

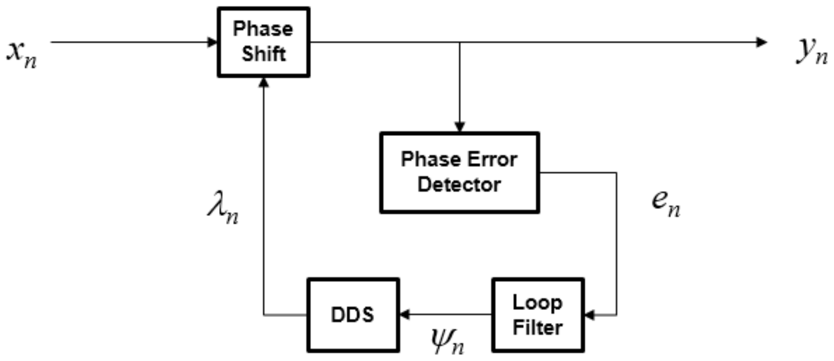

Figure 6-9: Block diagram of the carrier synchroniser which compensates for the frequency and phase offset of the carrier. [49]

with f_0 representing the emitted frequency of the symbol clock, Δv the relative speed of the source and receiver and c the velocity of the waves in the medium. As the maximum speed of the satellite is $4\,\mathrm{m\,s^{-1}}$, which relativity small to the speed of light, the effect will be minor. For the selected symbol rate of 400 MHz the maximum frequency shift for one OGS would be $\Delta f \approx 5\,\mathrm{Hz}$. As the positions of both OGSs are quite similar as seen from the satellite, this will result in a similar Doppler effect. The frequency offset of both signals will have small discrepancy and therefore will not influence the behaviour of the switching system. This knowledge combined with the heavy impact of the coarse frequency compensator on the memory usage for the simulation model is the reason for excluding this step in the synchronisation model.

The frequency and phase offset of the carrier is compensated using a closed-loop compensator [49]. The output of the compensator y_n is a frequency shifted version of the input x_n as in the following equation.

$$y_n = x_n e^{i\lambda_n} \tag{6-8}$$

with λ_n being the output of the direct digital synthesiser (DDS). The DDS can be seen as an integrator filter in this system. The phase error of the n^{th} symbol, e_n, is calculated using the following equation.

$$e_n = \mathrm{sgn}(\mathfrak{Re}\{x_n\}) \times \mathfrak{Im}\{x_n\} - \mathrm{sgn}(\mathfrak{Im}\{x_n\}) \times \mathfrak{Re}\{x_n\} \tag{6-9}$$

Stability is ensured by adding the following loop filter:

$$\psi_n = g_l e_n + \psi_{n-1},$$

with ψ_n the output of the filter and g_l the integrator gain. The output ψ_n is lead in the DDS:

$$\lambda_n = (g_p e_{n-1} + \psi_{n-1}) + \lambda_{n-1}.$$

The maximum pull-in frequency of the compensator can be calculated using the following equation:

$$(\Delta_f)_{pull-in} = (2\pi\sqrt{2}\zeta)B_n, \tag{6-10}$$

with B_n the normalized bandwidth and ζ the damping factor.

6-3-4 Symbol synchroniser

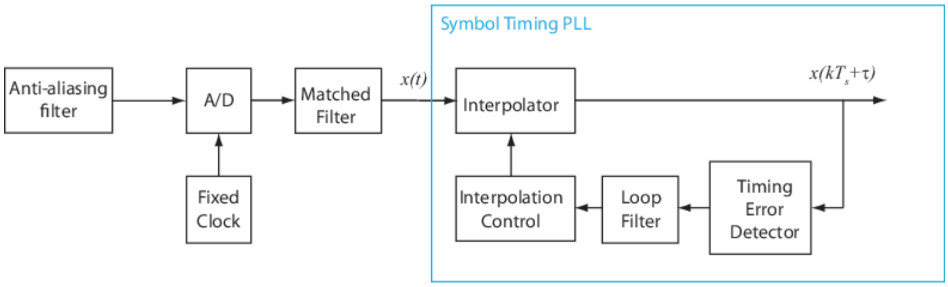

Figure 6-10: Block diagram of the symbol synchroniser which compensates for timing skew of the the samples. [49]

After the carrier synchronisation the receiver will synchronise to the signal symbols. To achieve this a phase-locked loop (PLL) algorithm is implemented. The algorithm consists of four parts [49].

- timing error detector (TED)
- interpolator
- interpolation controller
- loop filter

The timing error detection can be done using several techniques. The technique selected in this model is the Zero-Crossing method which is a decision directed method. Decision directed methods use the output of a symbol decoder to discipline and correct the timing error [57]. The timing error is calculated as follows [49]:

$$e(k) = x((k-1/2)T_s + \hat{\tau})[a_0(k-1) - a_0(k)] + y((k-1/2)T_s + \hat{\tau})[a_1(k-1) - a_1(k)], \quad (6\text{-}11)$$

with x and y are the in-phase and quadrature matched filter outputs, respectively. a_0 and a_1 coefficients are estimates of the $x(kT_s + \hat{\tau})$ and $y(kT_s + \hat{\tau})$, with $\hat{\tau}$ the timing error estimate [49].

The next step is the interpolator which is used to move the fixed rate samples to align the samples with the symbols of the signal. The interpolator is adaptive as the time-delay is unknown. The linear availability of the samples result in the characteristics of the output of a filter. In the used symbol synchroniser a piecewise parabolic interpolator with a Farrow structure and coefficient a set to 1/2 is implemented.

The interpolation controller provides the interpolator with the basepoint indexes, which are the nearest sample points, and the fractional interval which is the distance between the interpolant and the nearest basepoint.

The loop filter uses a PI controller with the following gains:

$$K_1 = \frac{-4\zeta\theta}{(1 + 2\zeta\theta + \theta^2)K_p} \quad (6\text{-}12)$$

$$K_2 = \frac{-4\theta^2}{(1 + 2\zeta\theta + \theta^2)K_p}, \quad (6\text{-}13)$$

with θ given by:

$$\theta = \frac{\frac{B_n T_s}{N}}{\zeta + \frac{1}{4\zeta}} \tag{6-14}$$

Where $N, \zeta, B_n T_s$ and K_p are defined as the number of samples per symbol, the damping factor, the normalized bandwidth and the detector gain, respectively [49].

6-3-5 Frame synchroniser

After the receiver is synchronised to the symbols the receiver will have to synchronise to the data contained in these symbols. Each PLFRAME has a header which is known to the receiver. The SOF of a DVB-S2 signal contains 26 symbols. The receiver tries to recognize the SOF by calculated the correlation of the received signal with the known sequence. The received signal in the input is complex, to compare the correlation values the absolute value is taken as the received signal could be 90/180/270 degrees out of phase. When the absolute correlation is higher than 50% the SOF is assumed to be recognised and the data of the next 32490 symbols will be buffered and sent out. At the same time a validate signal is sent to the data processor.

SFRAME

In case SFRAME is used it will be necessary to first recognise the SOSF to recollect the PLFRAMEs. The frame synchronisation uses the same principle. After synchronisation the SFRAME headers are removed and the PLFRAMEs are lead out to the next frame synchroniser.

The simulations done using SFRAMEs resulted in more errors. Due to the length of the SOSF correlation problems might occur. In the paper of De Gaudenzi [58] an alternative method is discussed which divides the SFRAME in several sub-blocks and uses multiple correlations to improve frame synchronisation. The implementation of SFRAMEs satellite communication will have to be further researched before we can include it in the seamless switching research.

6-3-6 Phase ambiguity corrector

After the SOFs are recognised these are used to solve the phase ambiguity. Phase ambiguity is the possibility of the modulated signal being out of phase by 90/180/270 degrees. The known SOF is compared to the received SOF. This is done using the following steps [49]:

1. The observed signal is expressed as $y(t) = x(t)e^{j\phi} + n(t), t = 1, 2, ..., N$
2. Define $y_1(t) = \overline{x}(t)y(t) = e^{j\phi} + \overline{x}(t)n(t)$. Where $\overline{x}(t)$ is the conjugate of signal $x(t)$. This is true as $\overline{x}(t)x(t) = 1$. The goal is to estimate the value ϕ from the observation $y_1(t), t = 1, 2, ...N$ i.e., estimate the value $B = e^{j\phi}$, and $\phi = \text{angle}(B)$
3. Suppose $n(t)$ yields to an independent and identically distributed complex AWGN distribution $N(0, \sigma^2)$. Then a non-biased estimator could be $B_{\text{est}} = \frac{1}{N}\sum(y_1(1:N))$, and $\phi_{est} = \text{angle}(B_{\text{est}})$ and the variance of B_{est} is σ^2/N.

The result of these steps will then be used to conclude how the signal will be altered.

- If $-\pi/4 < \phi_{est} < \pi/4$ the received signal is multiplied by e^{j0}.
- If $\pi/4 < \phi_{est} < \pi \cdot 3/4$ the received signal is multiplied by $e^{j\pi/2}$.
- If $\pi \cdot 3/4 < \phi_{est}$ or $\phi_{est} < -\pi \cdot 3/4$ the received signal is multiplied by $e^{-j\pi}$.
- If $-\pi \cdot 3/4 < \phi_{est} < -\pi/4$ the received signal is multiplied by $e^{-j\pi/2}$.

After this final synchronisation step the received signal is improved and structured during the whole synchronisation process. The signal is now ready for decoding.

6-4 Decoding

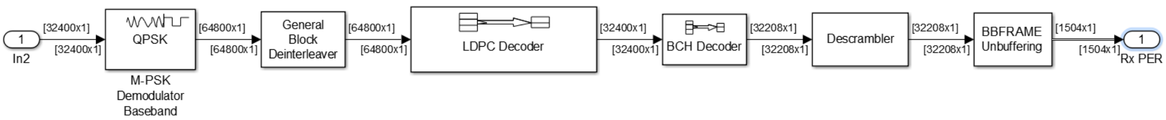

Figure 6-11: Overview of the decoding part of the receiver.

In the decoding part of the receiver the symbols are translated in the desired transmitted information. First the modulated signal will be demodulated and then the error correcting techniques are used to make sure the correct data is received. After this step the data will be evaluated to check if any errors occurred.

6-4-1 Demodulator

The demodulator reverses the handling of the modulator at the transmitter. The symbols as shown in Figure 6-3 are translated to bits. In the case of the simulation a QPSK modulated signal is used and therefore every symbol translates into two bits.

6-4-2 Deinterleaver

The deinterleaver reorders the received bits into the order as they were lead into the interleaver at the signal generator of the transmitter. For QPSK modulated signals the interleaver is switched off.

6-4-3 LDPC decoder

The LDPC decoder uses the log-likelihood to make decisions on the decoded bits. This is done be calculating the log likelihood ratio of every bit as shown in the following equation by [49].

$$L(c_i) = \log\left(\frac{(\Pr(c_i = 0|\text{channel output for } c_i)}{(\Pr(c_i = 1|\text{channel output for } c_i)}\right) \tag{6-15}$$

With c_i the i^{th} bit of the received codeword c. The algorithm uses three variable which are constantly updated during the iterations: $L(r_{ji}), L(q_{ij})$, and $L(Q_i)$. The initial value of $L(q_{ij})$ is $L(q_{ij}) = L(c_i)$. The updates occur using the following equations:

$$L(r_{ji}) = 2\,\text{atanh}\left(\prod_{i' \in V_j \setminus i} \tanh(\frac{1}{2}L(q_{i'j}))\right) \tag{6-16}$$

$$L(q_{ij}) = L(c_i) + \sum_{j' \in C_i \setminus j} L(r_{j'i}) \tag{6-17}$$

$$L(Q_i) = L(c_i) + \sum_{j' \in C_i} L(r_{j'i}) \tag{6-18}$$

With the set $C_i \setminus j$ is meant column $c_i = 1$ of matrix H minus the contribution of row j.

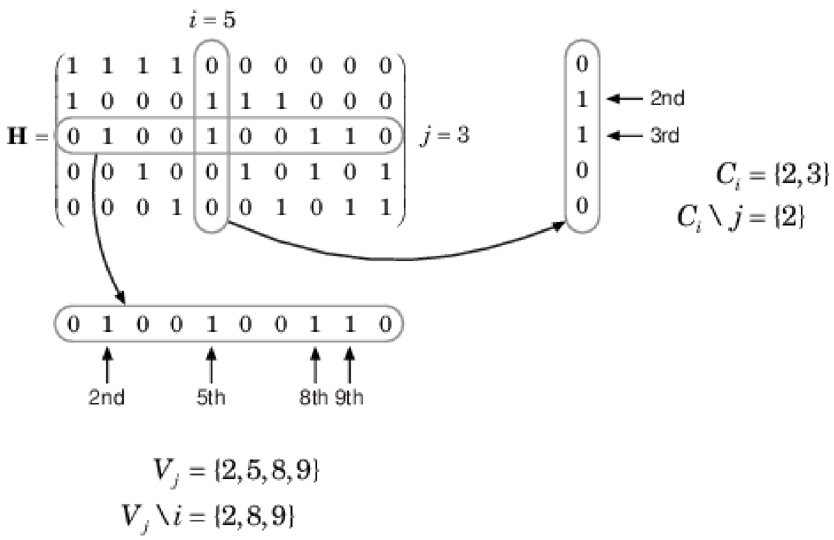

Figure 6-12: Method of index selection for LDPC decoding.

Analogically for the set of $V_j \setminus i$ of row j as seen in Figure 6-12. H is the parity check matrix as discussed in section 6-1-3. After every iteration $L(Q_i)$ provides an updated estimation of the value. After every iteration the code word is parity checked ($Hc^T = 0$). If the codeword is correct the iteration will stop and the decoded bits will be lead into the BCH decoder. If the parity check fails another iteration will be done until the maximum number, being set at 50, of iterations is done. If after 50 iterations the codeword still is not successfully decoded the frame the information can not be retrieved. The output of the decoder are frames of 32400 bits as the decoder is set to be hard-decision. If the decoder is set to be soft-decision the log-likelihood ratios would be put out.

6-4-4 BCH decoder

The algorithm of the BCH decoder checks if any errors are contained in the received frame. This is done by checking the first $2t$ terms of the infinite syndrome polynomial $S(z)$ [49].

$$S_i = \sum_{i=1}^{N} c_i \alpha^{N-1-i} \tag{6-19}$$

N is the length of the codeword, c_i is the value of the bit on the i^{th} position of the codeword and α is the primitive element of the Galois field of the code [49]. If these terms are equal to zero, there are no errors and the decoding of the data is finished. If one or more terms are non-zero the error locator polynomial $\Lambda(z)$ is calculated. This is done using the Berlekamp algorithm. The next step is to calculate the error evaluator polynomial, $\Omega(z)$, using the following equation:

$$\Lambda(z)S(z) = \Omega(z) \mod (z^{2t}) \tag{6-20}$$

An error in the codeword is then corrected using the result of this equation:

$$e_{i_m} = \frac{\Omega(a^{-i_m})}{\Lambda'(a^{-i_m})} \tag{6-21}$$

With e_{1_m} the error magnitude in the ${i_m}^{\text{th}}$ position in the codeword. the value of m is less than the error-correcting capability of the code, $\Omega(z)$ is the error magnitude polynomial, $\Lambda'(z)$ is the formal derivative of the error locator polynomial, $\Lambda(z)$ [59].

6-4-5 Descrambler

The descrambler does the inverse of the scrambler at the transmitter. The bits will be reordered in the same way as they were once generated at the transmitter. The BBFRAMEs are buffered in the size of the original MPEG packets and then sent to be evaluated.

6-5 Evaluation

The evaluation block is used to measure the performance of the applied time delay compensation. This is done by comparing the received data with the transmitted data. The comparison is done on two levels: the LDPC bits and the MPEG packets.

6-6 Measuring the timing difference

The biggest challenge in compensating the time delay is the lag time of the possible feedback. Therefore, as described in chapter 5, is chosen to use feed forward control. To achieve an optimal performance the disturbances on system have to be compensated for. The disturbances working on the system are measured by using a second parallel system. This parallel system is a downlink signal sent from the satellite towards the OGSs. The travelling time of the downlink signal will be equivalent to the travelling time of the uplink signal. By measuring the timing difference of the two downlink signals at the control centre the disturbances of the uplink are known.

The downlink signal is simulated using a random binary signal. The samplerate of the signal equals four times the symbolrate of the uplink. This is done to produce accurate measurements of the timing difference. The signal follows two paths. Each path is delayed by the same amount of steps as the uplink signals corresponding to OGS #1 and #2. The cross correlation of the two signals is then calculated and the maximum value is selected. Thereby estimating

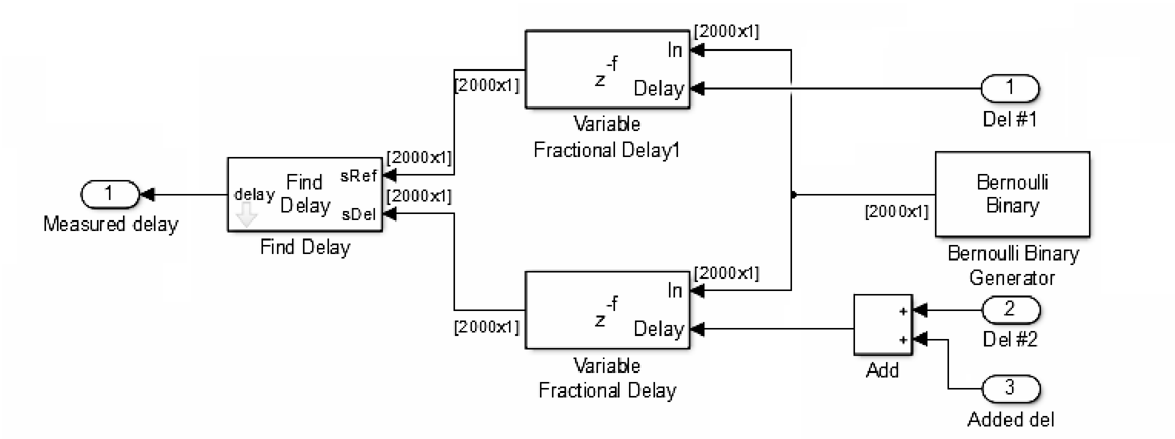

Figure 6-13: Overview of the measurement part which is added to acquire knowledge about the to be compensated time delays.

the timing difference of the two uplink signals. The correlation window in the simulation is 6000 steps which corresponds to a total measurable time difference of 1.9391 µs. The measured value is sent to the controller of the system to use in the compensation for the delay.

6-7 Time delay compensation

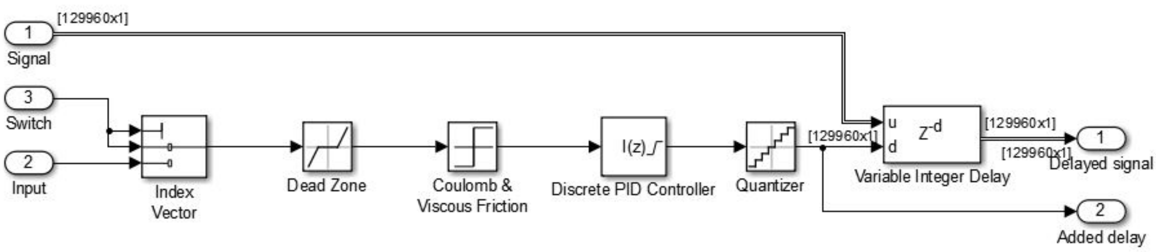

Figure 6-14: Overview of the controller part which is added to compensate the measured time delays.

In the simulation model only the time delay of one transmission channel is controlled. This is done as travelling time of the signal through OGS #1 takes more time than through OGS #2. To compensate for this difference a controlled time delay will be added to transmission channel #2. In a network of multiple OGSs it might be needed to equip every transmission channel with a controlled time delay.

To compensate for the measured time delay a concatenation of switches and delay lines is used as described in section 4-1. These delay lines will add a delay to the uplink of the OGS which will be used after the switch. In the simulation the different lengths of delay lines are represented by the quantised amount of added delay. The measured delay difference is used to acquire a setpoint for the controller. To create a robust controller, which is not too heavily influenced by corrupt measurements, an integrator is used. The controller only exists of an integrator as the concatenated switches and delay lines do not have dynamics. The integrator uses the forward Euler method and has a lower limit of 0 as it is not possible to add a negative time delay.

The integral combined with the quantised output of the controller is not stable as the error as a result of the quantisation combined with the integrator keep accumulating to the output of the controller as explained in section 5-3-1. To solve this a deadzone is added to the controller. If the measured delay difference is within half of the quantisation step no contribution will be done to the integral. The *Coulomb & Viscous Friction*-block is added to add an offset which compensates for the effect of the *Deadzone*.

The controller is switched off if the uplink signal passes through the corresponding OGS. This is done as altering the delay will corrupt the signal sent over the link. In the simulation only one of the links is compensated. In the real world system each link within the OGSs network will have to be equipped with an compensator.

6-8 Model validation

The validation of the simulation model is difficult. The fact that the model is capable of transmitting and receiving distorted signals, proofs the model is a valid communication model. The performance of the receiver is more difficult to class as the performance and used techniques of different modems can vary much. At this point not much is known of the quality of modems that will be used in future optical satellite links. Also the transmission channel conditions can have large variations. The wide variety of the system parameters make it impossible, at this moment, to validate the values for future systems.

The model can be used as an environment to test the behaviour of the time delay compensation system. These simulations and results are discussed in the next chapter. From the simulation performance results we can conclude if the proposed solution is feasible. Further research will be needed to make sure the used parameters of the model represent the real world conditions.

Chapter 7

Simulations and results

The model described in the previous chapter is used to investigate the behaviour of the proposed time delay compensation system. The goal of the simulations is to measure the performance of the system and use the results as a guideline for further studies. Most simulations are set to depict the worst case scenario. This is done to illustrate the effect of adding the time delay compensator. Simulations with the goal to depict real world situations are difficult to achieve as much is unknown of the future optical systems. Each simulation is done over a 10 s timespan which is very large compared to the short sample times of 0.624 ns. After every 50^{th} physical layer frames (PLFRAMEs) a switch is made between the two optical ground stations (OGSs). This equals a switch every 4.2 ms. In a simulation of 10 s 2381 switches will be made. The fast switching does not resemble the real world as only an approximate of 500 switches per year are planned. The fast switching is purely done to investigate the behaviour during switching. Unless stated otherwise, the channel conditions are shown in Table 7-1. The frequency offset is the same as the source of both channels is the same modulator. Doppler effects are neglected as the difference for both channels is too small. The parameters result in a signal-to-noise ratio (SNR) of ~ 5 or expressed in E_b/N_0 as $\sim$4 dB. E_b/N_0 is the ratio of bit energy to noise power spectral density [49].

In the first part of this chapter some baseline simulations are discussed to validate the system. The second part consist of more specified simulations to stretch the system to its performance limits.

	OGS #1	**OGS #2**
Phase offset	$-19°$	$109°$
Freq offset	-100 Hz	-100 Hz
AGWN	0.01	0.01
Path loss	10 dB	7 dB
SNR	~ 5.6	~ 5.2
E_b/N_0	$\sim$5 dB	$\sim$4.2 dB

Table 7-1: The parameters used in the simulations, unless stated otherwise.

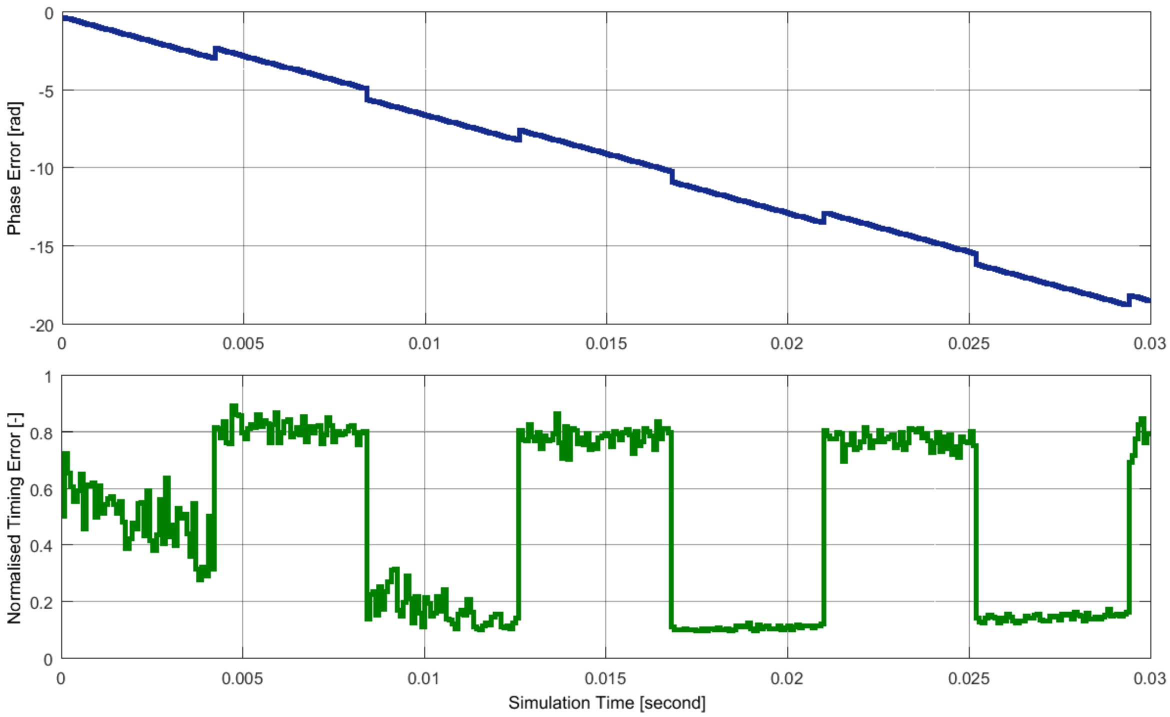

Figure 7-1: The estimated phase and timing errors are shown. The top graph show the phase error output of the frequency synchroniser and the bottom graph shows the normalised timing error estimations for the symbol synchroniser. Both graphs are smoothed by averaging the values over the PLFRAMEs.

7-1 Baseline simulations

The first simulation results show the capabilities of the system as a communication model. The standard situation is simulated, meaning clear-sky conditions and no need to switch between transmission channels. The movement of the satellite, the added white noise and the path loss does not prevent the system to receive any the data. Zero errors are incurred during a test of 10 s, transmitting and receiving ~7.7 Gbit.

Whenever errors occur it is mostly 22 packets at a time, which equals the length of a PLFRAME. The reason might be that frame synchronisation has failed a result of an unrecognised start of frame (SOF). The SOF is the part of a packet most affected by the switching due to the placement at the beginning of a PLFRAME. The Figure 7-1 show the estimated phase errors. The phase error according to the frequency synchroniser in the top graph shows an expected result. The linear shape corresponds to the frequency offset of the channel. As a result the phase error is constantly growing. The sudden shifts correspond to the switches between the OGSs. The shifts are a result of the different phase offsets. The bottom graph shows the normalised timing error of the symbol synchroniser. The switch between the two links are easily to spot. The timing for the two links differ as a result of the phase offset and time delays. At the beginning of the simulation the timing error decreases. Afterwards the two values are stable. The reason for this is unknown but might be a result of the feedback loop of the symbol synchroniser. The next simulation is used to find the limits

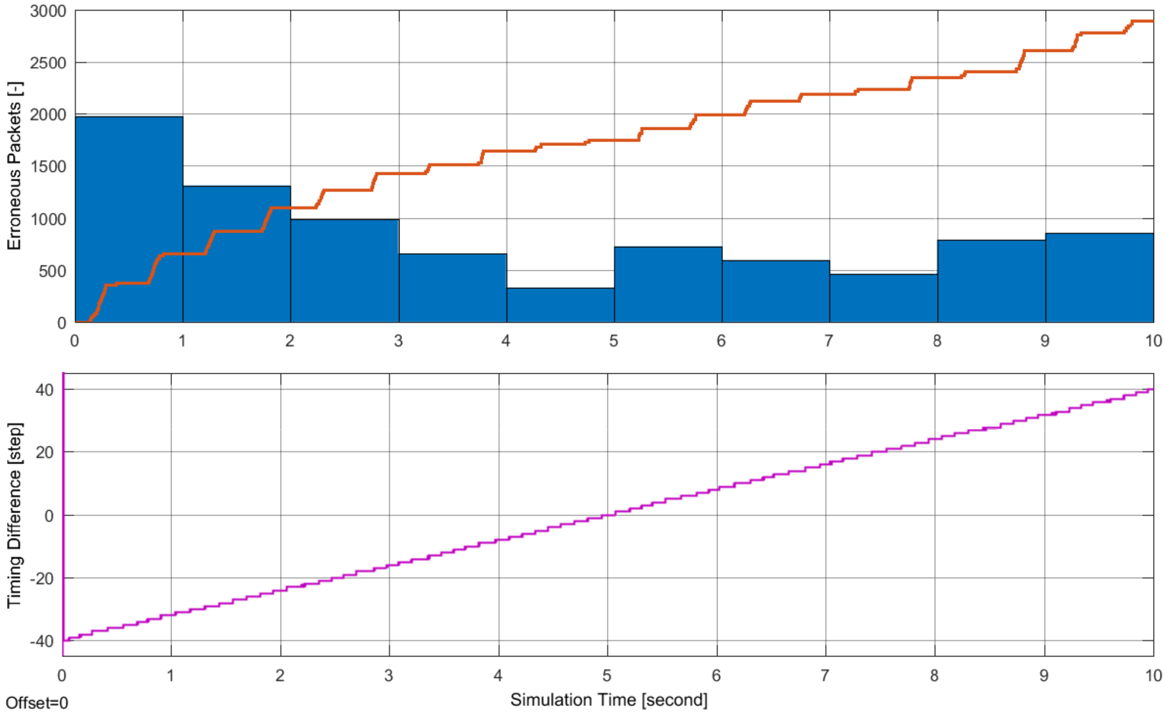

Figure 7-2: Packet error compared to the timing difference. The bottom graph shows the timing difference of the two OGSs. Negative values represent a delayed line for OGS #2 and positive values an delay for OGS #2. The red line in the top graph shows the cumulative number of packet errors and the blue bars show the number of packet errors per second. The values of the bar are tripled to improve visualisation.

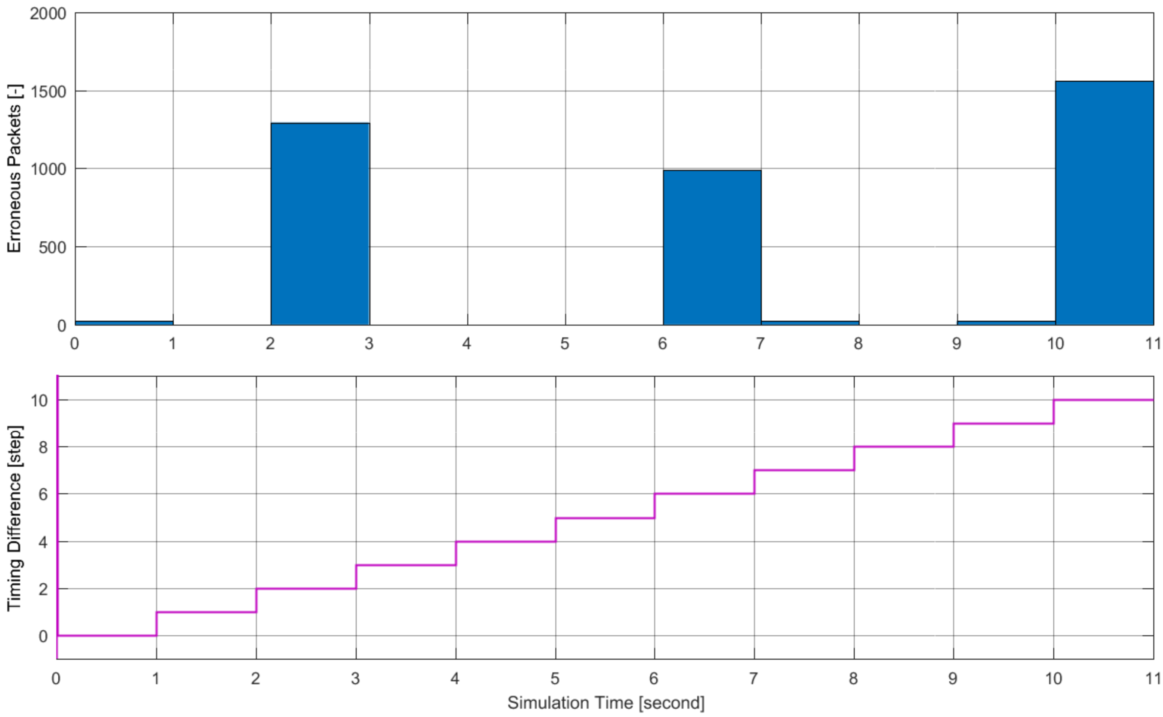

Figure 7-3: Number of erroneous packets per timing difference between the different OGSs. The errors occur at timing difference that is equal to half a symbol as there are 4 samples per symbol.

of the switching system without being influenced by the time delay compensator. This is achieved by setting the precision to 100 steps, so it will not be able to compensate for the small time delay changes. The simulation starts with an extra time delay difference of 40 steps for OGS #2. During 10 s of simulation the time delay difference moves gradually to an extra time delay difference of 40 steps for OGS #1. In Figure 7-2 the number of packet errors compared to timing difference is shown. The graph shows a quite symmetrical behaviour as the most errors occur at the beginning and the end of the simulation. This is a logical result of the simulation model as the switches are made back and forth. The delay direction should therefore have no influence on the results. The symmetrical shape confirms this. Nevertheless there is a small difference in the amount of packet errors at the beginning and end of the simulation. The reason could be the dynamics of the system as the timing difference is decreasing in the first half of the simulation and growing at the second half.

Halfway the simulation the time delay difference is zero. The system should then be able to receive the signal without any problem. Nevertheless the results show that within this region some packets are not received properly. This might be because the time delay is changing to fast and the receiver has difficulties to lock onto the signal. Another noticeable behaviour is that the errors are clustered. The period between the clusters is 4 samples, which corresponds to the number of samples per symbol. The clusters are bigger when the timing difference is large. The reason for this could be the loss of several symbols, which challenges the frame synchroniser to recognise the SOF. To allow the receiver to achieve a better lock on the signal another simulation has been done which changes the time delay difference in steps.

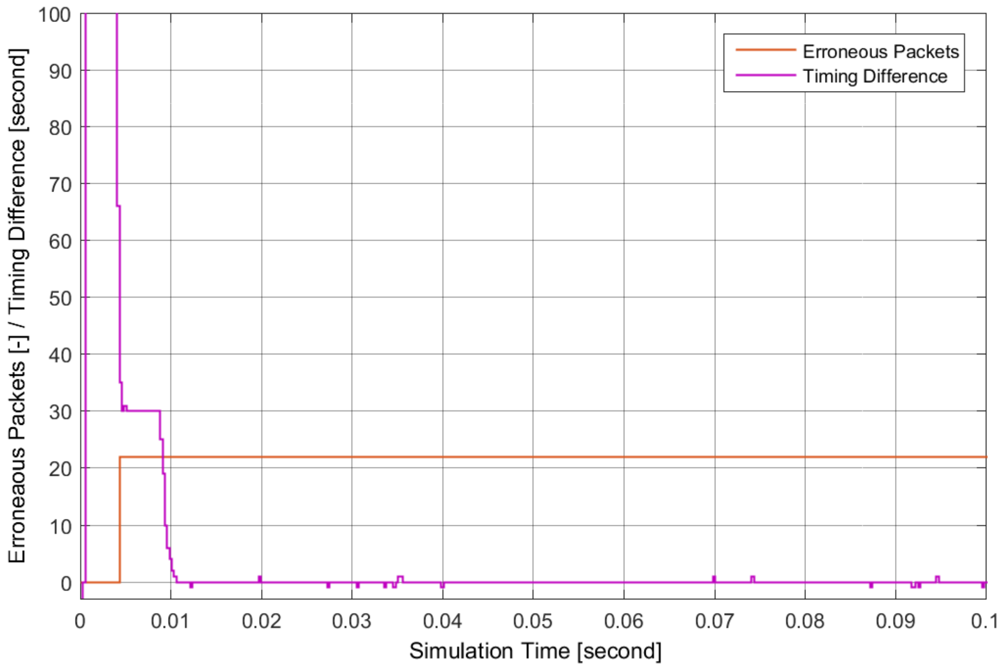

Figure 7-4: The start of time delay compensation. The first switch is made at $4.2\,\mathrm{ms}$ when the timing difference is ∼30 steps. The compensation system is therefore paused and proceeds towards zero timing difference after the next switch at $8.4\,\mathrm{ms}$. The red line shows the number of erroneous packets.

The results are shown in Figure 7-3. The system has troubles receiving the data whenever the timing difference equals 2, 6, 10 samples. These numbers translate to a modulus 4 timing difference of 2 samples which correspond to half a symbol as the number of samples per symbol is 4. This could be a result of the symbol synchroniser having difficulties to lock. The number of samples differ by half a symbol which results in the symbol synchroniser to be challenged by the worst case scenario. The symbol synchroniser will receive samples exactly in between two symbols. This can be visualised in Figure 6-8b as samples being received in between the four clusters. The performance of the Digital Video Broadcasting - Satellite 2nd generation (DVB-S2) receiver depends on the system parameters. Real world tests will be needed to conclude if half symbol timing differences indeed cause such errors. The errors at zero timing difference is a result of the slow rise time of the controller. As can be seen in Figure 7-4. The large timing difference is quickly compensated in the beginning. At $4.2\,\mathrm{ms}$ the first switch is made which halts the time delay compensator. At $8.4\,\mathrm{ms}$ the link switches back to OGS #1 and the compensator continues to reduce the timing difference. The lack in speed of the controller results in the loss of one PLFRAME, containing 22 packets. This could be solved by tuning the controller parameters if more speed would be needed in the eventual system. We assume it will not be necessary to achieve these fast switches.

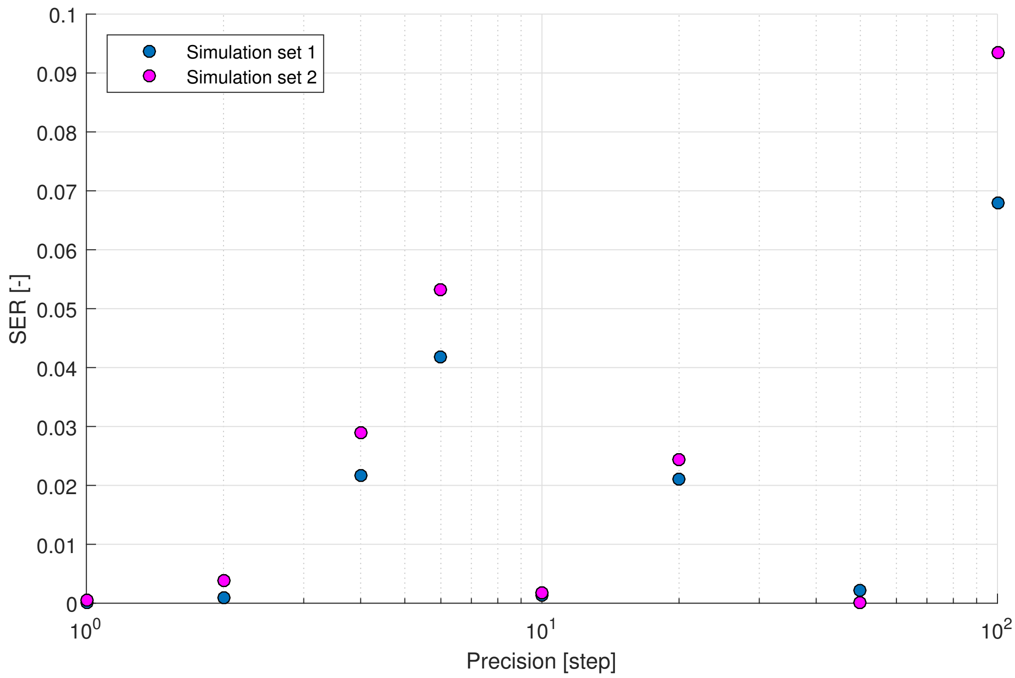

Figure 7-5: Scenario simulations performances

7-2 Scenario simulations

The next step is to simulate scenarios which could occur in the real world. The satellite movement is considered and the time delay compensator is enabled. The satellite movement is centred around the worst case scenario where the time delay is in between two delay steps of the time delay compensator. For instance the time delay difference is set around 755 steps when the precision of the time delays is set at 10 steps and thus the closest possible compensation settings are at 750 and 760 steps. The worst case scenario will set a lower performance limit as the real scenario will have similar or better results.

Eight different scenarios are simulated and repeated. The scenarios vary in the precision of the compensator as can be seen in table 7-2. For every precision there are two different simulations containing different phase offset between the signals. The first set of simulations has a phase difference of 84° and the second set 128° Every simulation describes a 10 second time frame and during the simulation after every 50 PLFRAMEs the OGS was switched. The total amount of switches during a 10 seconds simulation is 2381.

We define the number of switches that causes an error divided by the total number of switches as the switch-error rate (SER). Overall the SER increases when the compensator is set to be less precise. Nevertheless there are surprising results for the precision of 10 and 50 samples. Especially for the scenario where the precision is 50 samples and the time delay compensation is off by ~ 25 samples translating into 6 symbols. As the SOF consists of only 26 symbols you would expect to heavily impact the frame synchronisation. A possible explanation will be discussed later on in this section. Simulations of set 1 have a slightly better performance than the simulations of set 2. The reason for this could be the larger phase difference which

Scenario	Precision (Δ)	SER #1	SER #2
#1	1 sample	0	4.2e−4
#2	2 samples	8.4e−4	3.7e−3
#3	4 samples	2.1e−2	2.9e−2
#4	6 samples	4.1e−2	5.3e−2
#5	10 samples	1.3e−3	1.7e−3
#6	20 samples	2.1e−2	2.4e−2
#7	50 samples	2.1e−3	0
#8	100 samples	6.8e−2	9.4e−2

Table 7-2: Scenario simulations. The SER is the rate of switches that causes an error compared to the total number of switches.

make it more difficult for the receiver loops to adjust.

Several simulations are depicted in Figure 7-6. The timing difference for the larger precision simulations show the delay line switches clearly. The first is at ∼1.6 s and changes the direction of the timing difference. Except for the influence of those switches, the sine function which depicts the satellite movement is easily recognised. Most simulations show similar results as the errors occur during the steepest change in time delay. It could be that the synchronisation loops are stretched in these situations resulting in errors. With the loops being stretched is meant that the constant change in delay causes the loops to adjust and therefore reaching the limits of the performance. This reasoning however does not explain the double step which is shown in Figure 7-6c for the simulation with a precision of 6 steps. In that simulation no errors occurred in the steepest part of the timing difference.

As we look to the graphs in more detail the error clusters correspond to timing differences that correspond to modulo 4 resulting in a remainder of 2. Using Figure 7-3 we can try to explain this behaviour. We conclude from this that the symbol synchroniser is the most important reason for the errors. The timing difference has an influence on the size of the error cluster. As the difference will result in more symbol losses which challenges the frame synchronisation more severe. It is thus important that the timing difference will be held to a minimum.

We know get back to the simulation with the 50 steps precision. The timing difference fluctuates at 25 steps and below. The modulo 4 of 25 is 1 which corresponds to the results of a timing difference of 5 steps in Figure 7-3 of the baseline simulations. The setup of the satellite movement of the simulation prohibits the timing difference to hit numbers with a corresponding modulo 4 resulting in 2 which causes the receiver to lock out. As a result the exceptional performance in these simulations are based on a coincidence; a different satellite movement than the one used in this simulation might give different results.

Simulations with a time delay compensator precision of 200 were unsuccessful. In Figure 7-7 an attempt is shown. After 3.1 seconds the receiver fails to lock on to the signal and is unable to recover. This results in zero successful transmitted bits from that point on. The overlap of $\sim$ 50 symbols might perturb the loops in the receiver to heavily. Therefore these simulations are not further considered.

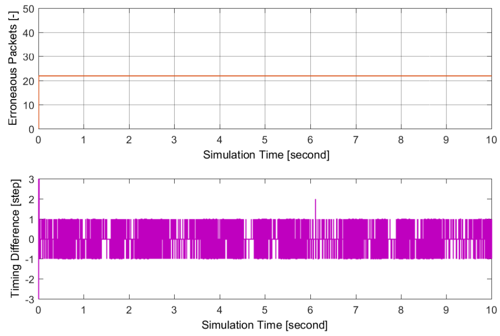

(a) Performance of simulation with precision of 1.

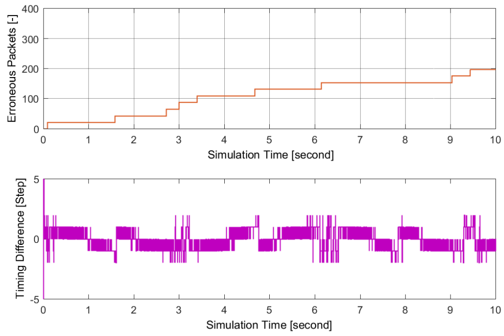

(b) Performance of simulation with precision of 2.

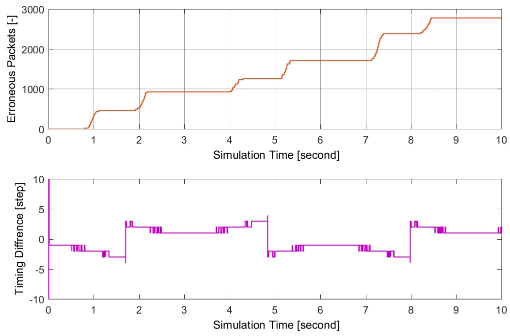

(c) Performance of simulation with precision of 6.

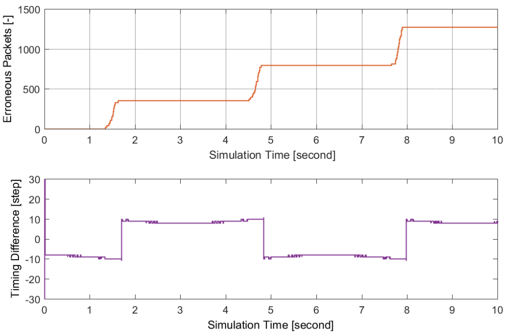

(d) Performance of simulation with precision of 20.

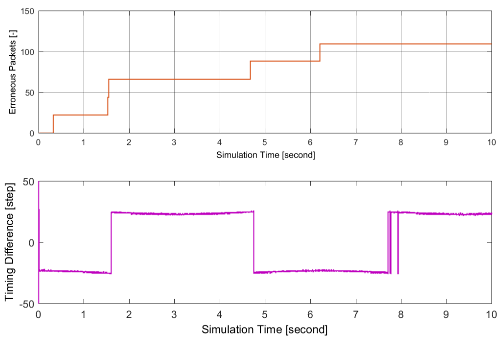

(e) Performance of simulation with precision of 50.

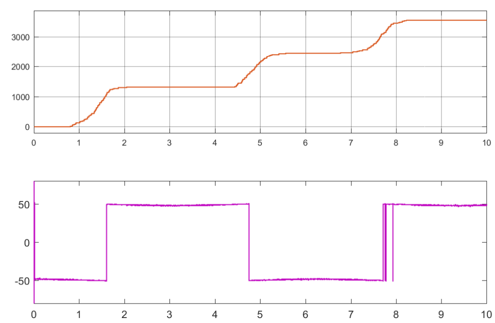

(f) Performance of simulation with precision of 100.

Figure 7-6: Scenario simulations

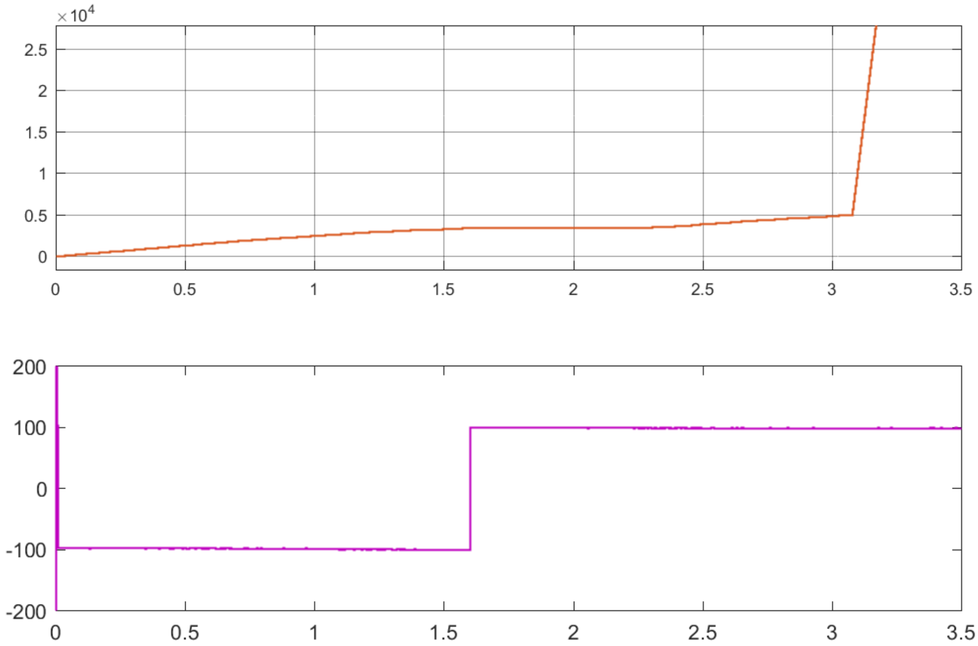

Figure 7-7: Performance of simulation with precision of 100. After 3.1 seconds the receiver fails to lock.

7-2-1 Upsampling

The errorless result for the simulation with precision 1 could be a consequence of rounding in the simulation. To test if the effect of rounding in the simulation process influences the performance another test is done. The simulation is repeated with upsampling of 8 instead of 4. The precision of the is time delay compensator is set at 2 samples to resemble the precision of a quarter of a symbol. The test showed the same flawless result. We conclude from this that the precision of a quarter of a symbol is indeed sufficient.

7-2-2 Use of super frames (SFRAMEs)

As discussed in section 2-3-1 the implementation of SFRAMEs can be necessary to control the switching at the satellite. Therefore a simulation model is built including the use of SFRAMEs. The method of frame synchronisation was not changed during these simulations which led to more errors during the simulations. The reason for this is that the frame synchronisation method is specialised on recognising SOFs of 26 symbols. For start of super frames (SOSFs) containing 270 symbols more advanced synchronisation techniques might be needed, which are now under research [58]. As much is still unknown about the implementation of SFRAMEs, resulting in bad and unrepresentative performances of the receiver, the simulations are excluded from the results.

7-3 Results interpretation

The SERs resulting from the simulations differ between 0 and 10% for precisions up to 100 steps. Even when the overlap between the two signals is 25 symbols 90% of the switches will be seamless. Translating this number to the assumed 500 switches per year, 50 PLFRAMEs will be lost over that period of time. This fits well within the promised link availability of SES. But to assure seamless switching every time, a precision of a quarter of a symbol time will be needed. As this will result in a low phase difference between the two signals. A large phase difference causes the symbol synchroniser to lock out, resulting in packet losses. The conclusion that the accuracy of a quarter of a symbol is sufficient for good performance proves that the technique of concatenated delay lines can fulfil the requirements of the variable photonic delay line (VPDL) in the time delay compensator.

In the simulation model a quarter of a symbol has a sample time of 0.646 35 ns. The total time delay range of the compensator should be 10 µs. If binary switches are used the required amount is 14 as this results in 16384 time delay settings. When three branches per switch are used, 9 switches will suffice to reach a time delay range of $19683 \cdot 0.64635\,\text{ns} = 12.7221\,\mu\text{s}$.

Chapter 8

Conclusions and Recommendations

To conclude the thesis the results are discussed according to the sub questions stated in section 1-1. From the individual answers the conclusion will be derived if the main objective of the thesis is achieved and a valid solution is proposed to solve the problem of seamless switching.

In chapter 2 the requirements of an optical feederlink are discussed. A feederlink provides the geostationary satellite with all the data that is transmitted from the satellite. For an optical feederlink the radio frequencies (RF) satellite dishes are replaced by telescopes. To ensure link availability it will be necessary to switch between optical ground stations (OGSs) in a network of ~ 10. The method of transmitting the optical is still being discussed. At this moment transparent transmission is chosen, being digital or analogue transparent. To continue research on the seamless switching it will be necessary to first get a clearer image of the to be chosen techniques for a ground-to-GEO link. This will change parameters and possibly modulation methods. The simulation model can be made much more accurate using values applicable to chosen techniques. Implementation of SFRAME in the Digital Video Broadcasting - Satellite 2nd generation (DVB-S2) signal could enable the switching control on the satellite. The header can contain information about which OGS to switch to. The second telescope on the satellite can then align with the OGS and start the synchronisation process. The implementation of super frames (SFRAMEs) enable also the use of dummy frames, thereby prohibiting the loss of valuable data. More research is needed on the implementation of SFRAMEs as much is uncertain about the performance at the moment.

Synchronisation should be done on the ground, as the processing power on a satellite is limited and the complexity should be held at a minimum. The chosen strategy for synchronisation is thus to use one modulator and multiple dedicated terrestrial links to connect to the OGSs in the network. It will be necessary to have at least two telescopes on the satellite to perform a seamless switch as changing the aim from one OGS to another will take to long. Using one modulator ensures the two link signals will be very similar. The travelling time difference of the links via the two OGSs will be compensated using a variable photonic delay line (VPDL). The length of the delay line is set using measurements on a parallel system. This system is a downlink signal from the satellite towards both OGSs and through the same terrestrial links.

The timing difference is then measured at the control centre where the modulator is based. The measurements are used to set the length of the delay line. Thereby equalising the path lengths of the two links and synchronising the signals. When the links are perfectly aligned a switch can be made at the modulator and thereby changing the transmitting OGS.

Currently existing VPDLs are limited in either bandwidth or time delay range. Both are important requirements for the optical feederlink. The only fully working option is a concatenation of switches and delay lines. The lack of continuous precision is a disadvantage but will not prohibit the time delay compensator system from functioning. Future research will be needed to mature the other VPDL techniques and thereby enabling continuous precision of the time delay compensator, thereby further improving the performance.

The system will use feed forward control to steer the VPDL. The knowledge about the disturbances is measured using a parallel system which consist of a downlink signal. This method bypasses the otherwise long feedback delay of at least 250 ms. The disturbances consist of the satellite movement and the atmospheric turbulences. An integrator combined with a deadzone and a quantiser is used as the controller. Thereby converging the system to the optimal settings of the concatenated delay lines.

The simulation model in *Simulink* works and represents a valid communication system. During the simulations the worst case scenario for every precision of the time delay compensator was tested to set a lower performance limit. The most sensitive part of the receiver looks to be the symbol synchroniser. When the symbol timing is off by half a symbol errors occur. The number of errors depends on the number of symbols lost due to overlapping of the two signals. To ensure seamless switching in the simulation model a precision of a quarter of a symbol time is needed. To achieve this precision combined with a time delay range of 10 µs 14 binary switches or 9 switches with three branches are needed. This type of VPDL is thus proven to be sufficient enough to synchronise the OGSs. Even if the precision is less good the number of packet losses is limited. A precision time of 25 symbols still has a 90% success rate. A failed switch only results in the loss of 1 physical layer frame (PLFRAME).

The parameters and performance of the system will have to be evaluated in the future. Thereby checking if the simulation model represents a valid real world system. There exists a wide variety of receivers and it will be important to check all the different possible techniques and settings to ensure the shown performance of the proposed system is valid. Further research will have to include more efficient modulation codes. In the simulation only the conservative QPSK-1/2 modulation is used. Nevertheless the simulations show that the time delay compensator has a positive result on the success rate of the switches. If the switches will be seamless with existing DVB-S2 receivers, as resulted in the simulations, will have to be proven by extensive testing.

At this point in time the proposed solution is promising and could be able to provide the necessary seamless switching for site diversity in optical ground-to-GEO links. However further research and development will be needed to validate the simulation results in the real world.

Bibliography

[1] J. N. Pelton, *Handbook of Satellite Applications*, ch. History of Satellite Communications, pp. 27–66. New York, NY: Springer New York, 2013.

[2] "SES-website." www.ses.com, 2015.

[3] A. Gharanjik, K. Liolis, M. Shankar, and B. Ottersten, "Spatial multiplexing in optical feeder links for high throughput satellites," in *Signal and Information Processing (GlobalSIP), 2014 IEEE Global Conference on*, pp. 1112–1116, Dec 2014.

[4] I. I. Kim, B. McArthur, and E. Korevaar, "Comparison of laser beam propagation at 785 nm and 1550 nm in fog and haze for optical wireless communications," in *proc. SPIE*, vol. 4214, pp. 26–37, 2001.

[5] D. Giggenbach, J. Poliak, R. Mata-Calvo, C. Fuchs, N. Perlot, R. Freund, and T. Richter, "Preliminary results of terabit-per-second long-range free-space optical transmission experiment thrust," 2015.

[6] J. Poliak, D. Giggenbach, F. Moll, F. Rein, C. Fuchs, and R. Calvo, "Terabit-throughput geo satellite optical feeder link testbed," in *Telecommunications (ConTEL), 2015 13th International Conference on*, pp. 1–5, July 2015.

[7] G. Foschini, L. Greenstein, and G. Vannucci, "Noncoherent detection of coherent lightwave signals corrupted by phase noise," *Communications, IEEE Transactions on*, vol. 36, pp. 306–314, Mar 1988.

[8] A. Morello and V. Mignone, "DVB-S2: The second generation standard for satellite broad-band services," *Proceedings of the IEEE*, vol. 94, pp. 210–227, Jan 2006.

[9] ETSI, *Digital Video Broadcasting (DVB); Second generation framing structure, channel coding and modulation systems for Broadcasting, Interactive Services, News Gathering and other broadband satellite applications; Part 2: DVB-S2 Extensions (DVB-S2X) EUROPEAN STANDARD* . ETSI, v1.1.1 ed.

[10] y. Agilent Technologies, "DVB-S2 baseband verification library."

[11] F. M. Gardner, "A BPSK/QPSK timing-error detector for sampled receivers," *Communications, IEEE Transactions on*, vol. 34, pp. 423–429, May 1986.

[12] G. Albertazzi, S. Cioni, G. Corazza, M. Neri, R. Pedone, P. Salmi, A. Vanelli-Coralli, and M. Villanti, "On the adaptive dvb-s2 physical layer: design and performance," *Wireless Communications, IEEE*, vol. 12, pp. 62–68, Dec 2005.

[13] U. Mengali and M. Morelli, "Data-aided frequency estimation for burst digital transmission," *Communications, IEEE Transactions on*, vol. 45, pp. 23–25, Jan 1997.

[14] J. Yao, "Microwave photonics," *Lightwave Technology, Journal of*, vol. 27, pp. 314–335, Feb 2009.

[15] L. Liao, D. Samara-Rubio, M. Morse, A. Liu, D. Hodge, D. Rubin, U. D. Keil, and T. Franck, "High speed silicon mach-zehnder modulator," *Opt. Express*, vol. 13, pp. 3129–3135, Apr 2005.

[16] Cisco systems, "Introduction to DWDM technology."

[17] ITU, "G.694.1 : Spectral grids for wdm applications: DWDM frequency grid," 2012.

[18] H. Song and M. Brandt-Pearce, "A 2-d discrete-time model of physical impairments in wavelength-division multiplexing systems," *J. Lightwave Technol.*, vol. 30, pp. 713–726, Mar 2012.

[19] F. Dios, J. A. Rubio, A. Rodríguez, and A. Comerón, "Scintillation and beam-wander analysis in an optical ground station-satellite uplink," *Appl. Opt.*, vol. 43, pp. 3866–3873, Jul 2004.

[20] D. Giggenbach and H. Henniger, "Fading-loss assessment in atmospheric free-space optical communication links with on-off keying," *Optical Engineering*, vol. 47, no. 4, pp. 046001–046001–6, 2008.

[21] R. Barrios and F. Dios, "Exponentiated weibull distribution family under aperture averaging for gaussian beam waves," *Opt. Express*, vol. 20, pp. 13055–13064, Jun 2012.

[22] R. Fante, "Electromagnetic beam propagation in turbulent media," *Proceedings of the IEEE*, vol. 63, pp. 1669–1692, Dec 1975.

[23] A. Belmonte, "Feasibility study for the simulation of beam propagation: consideration of coherent lidar performance," *Appl. Opt.*, vol. 39, pp. 5426–5445, Oct 2000.

[24] X. Zhu and J. M. Kahn, "Free-space optical communication through atmospheric turbulence channels," *Communications, IEEE Transactions on*, vol. 50, no. 8, pp. 1293–1300, 2002.

[25] C. Fuchs and F. Moll, "Ground station network optimization for space-to-ground optical communication links," *J. Opt. Commun. Netw.*, vol. 7, pp. 1148–1159, Dec 2015.

[26] "Flight dynamics department SES," 2015.

[27] DEV systemtechnik, "Ka-band diversity," 2015.

[28] S. Cioni, C. Niebla, G. Granados, S. Scalise, A. Vanelli-Coralli, and M. Castro, "Advanced fade countermeasures for DVB-S2 systems in railway scenarios," *EURASIP Journal on Wireless Communications and Networking*, vol. 2007, no. 1, p. 049718, 2007.

[29] J. Minet, M. A. Vorontsov, E. Polnau, and D. Dolfi, "Enhanced correlation of received power-signal fluctuations in bidirectional optical links," *Journal of Optics*, vol. 15, no. 2, p. 022401, 2013.

[30] C. Fuchs and F. Moll, "Ground station network optimization for space-to-ground optical communication links," *Optical Communications and Networking, IEEE/OSA Journal of*, vol. 7, pp. 1148–1159, Dec 2015.

[31] A. P. Goutzoulls, D. K. Davies, and J. M. Zomp, "Prototype binary fiber optic delay line," *Optical Engineering*, vol. 28, no. 11, pp. 281193–281193–, 1989.

[32] X. Li, J. Chen, S. Li, and Z. Hong, *Digitally Fast Programmable Optical Signal Processing Devices.* INTECH Open Access Publisher, 2009.

[33] Álvaro Rosa, A. Gutiérrez, A. Brimont, A. Griol, and P. Sanchis, "High performace silicon 2x2 optical switch based on a thermo-optically tunable multimode interference coupler and efficient electrodes," *Opt. Express*, vol. 24, pp. 191–198, Jan 2016.

[34] N. Madamopoulos and N. A. Riza, "Demonstration of an all-digital 7-bit 33-channel photonic delay line for phased-array radars," *Appl. Opt.*, vol. 39, pp. 4168–4181, Aug 2000.

[35] S. Fathpour and N. A. Riza, "Silicon-photonics-based wideband radar beamforming: basic design," *Optical Engineering*, vol. 49, no. 1, pp. 018201–018201–7, 2010.

[36] Y. Dai, X. Chen, Y. Okawachi, A. C. Turner-Foster, M. A. Foster, M. Lipson, A. L. Gaeta, and C. Xu, "1 μs tunable delay using parametric mixing and optical phase conjugation in si waveguides: reply," *Opt. Express*, vol. 17, pp. 16029–16031, Aug 2009.

[37] S. Chin and L. Thevenaz, "Tunable photonic delay lines in optical fibers," *Laser & Photonics Reviews*, vol. 6, no. 6, pp. 724–738, 2012.

[38] Y. Dai, Y. Okawachi, A. C. Turner-Foster, M. Lipson, A. L. Gaeta, and C. Xu, "Ultralong continuously tunable parametric delays via a cascading discrete stage," *Opt. Express*, vol. 18, pp. 333–339, Jan 2010.

[39] N. A. Riza, S. A. Reza, and P. J. Marraccini, "Electronically controlled agile lens-based broadband variable photonic delay line for photonic and radio frequency signal processing," *Appl. Opt.*, vol. 49, pp. 6718–6725, Dec 2010.

[40] N. A. Riza, "Switchless hybrid analog-digital variable optical delay line for radio frequency signal processing," *Optical Engineering*, vol. 48, no. 3, pp. 035005–035005–4, 2009.

[41] N. Primero, *Generation and application of dynamic gratings in optical fibers using stimulated Brillouin scattering.* PhD thesis, École Polytechnique Fédérale de Lausanne, 2013.

[42] K.-Y. Song, "Brillouin dynamic grating in optical fibers and its applications," in *Asia Communications and Photonics*, pp. 763008–763008, International Society for Optics and Photonics, 2009.

[43] N. A. Riza, M. A. Arain, and S. Khan, "Hybrid analog-digital variable fiber-optic delay line," *Lightwave Technology, Journal of*, vol. 22, pp. 619–624, Feb 2004.

[44] J. Li, R. Wang, R. Wang, Z. Xu, and Y. Su, "Novel large negative dispersion photonic crystal fiber for dispersion compensation," in *Mechanic Automation and Control Engineering (MACE), 2011 Second International Conference on*, pp. 1443–1446, July 2011.

[45] Y. Antman, L. Yaron, T. Langer, M. Tur, and A. Zadok, "Variable delay of gbit/s data using coded brillouin dynamic gratings," 2014.

[46] A. Meijerink, C. Roeloffzen, R. Meijerink, L. Zhuang, D. Marpaung, M. Bentum, M. Burla, J. Verpoorte, P. Jorna, A. Hulzinga, and W. van Etten, "Novel ring resonator-based integrated photonic beamformer for broadband phased array receive antennas 2014;part i: Design and performance analysis," *Lightwave Technology, Journal of*, vol. 28, pp. 3–18, Jan 2010.

[47] R. Tucker, P.-C. Ku, and C. Chang-Hasnain, "Slow-light optical buffers: capabilities and fundamental limitations," *Lightwave Technology, Journal of*, vol. 23, pp. 4046–4066, Dec 2005.

[48] B. Roffel and B. H. Betlem, *Advanced practical process control*. Springer, 2004.

[49] Mathworks, *Mathworks documentation database*. http://nl.mathworks.com/help/.

[50] A. B. S. Bahman Azarbad, "DVB-S2 model in matlab: Issues and impairments." http://nl.mathworks.com/help/comm/examples/qpsk-transmitter-and-receiver-1.html.

[51] Mathworks, "QPSK transmitter and receiver." http://nl.mathworks.com/help/comm/examples/qpsk-transmitter-and-receiver-1.html.

[52] J. Grotz, "Former employee Newtec," March 2016.

[53] Y. S. Han, "Bch codes."

[54] R. Gallager, "Low-density parity-check codes," *IRE Transactions on Information Theory*, vol. 8, pp. 21–28, January 1962.

[55] J. K. Wolf, "An introduction to error correcting codes." http://circuit.ucsd.edu/ yhk/ece154c-spr15/ErrorCorrectionIII.pdf.

[56] G. N. Gibson, J. Heyman, J. Lugten, W. Fitelson, and C. H. Townes, "Optical path length fluctuations in the atmosphere," *Appl. Opt.*, vol. 23, pp. 4383–4389, Dec 1984.

[57] H. Meyr, M. Moeneclaey, and S. A. Fechtel, *Digital Communication Receivers: Synchronization, Channel Estimation, and Signal Processing*. John Wiley & Sons, Inc., 1998.

[58] C. Rohde, N. Alagha, R. De Gaudenzi, H. Stadali, and G. Mocker, "Super-framing: a powerful physical layer frame structure for next generation satellite broadband systems," *International Journal of Satellite Communications and Networking*, vol. 34, no. 3, pp. 413–438, 2016.

[59] S. B. Wicker, *Error Control Systems for Digital Communication and Storage.* Upper Saddle River, NJ, USA: Prentice-Hall, Inc., 1995.

Glossary

List of Acronyms

ACM	adaptive coding and modulation
AGC	automatic gain controller
AWGN	additive white Gaussian noise
BBFRAME	base-band frame
BCH	Bose and Ray-Chaudhuri
CSI	channel state information
DBG	dynamic Brillouin grating
DDS	direct digital synthesiser
DLR	Deutsches Zentrum für Luft- und Raumfahrt
DVB-S2	Digital Video Broadcasting - Satellite 2nd generation
DWDM	dense wavelength-division multiplexing
ECVFL	electronically controlled variable focus lens
EDFA	erbium doped fiber amplifier
FEC	forward error correction
GVD	group velocity dispersion
HDF	high-dispersion fiber
HTS	high throughput satellite
IRT	index-of-refraction turbulences
ISI	inter symbol interference

ITU	International Telecommunication Union
LDPC	low-density parity-check code
ML	maximum-likelihood
MODCOD	modulation and coding
NLS	nonlinear Schrödinger
OGS	optical ground station
OOK	on-off keying
PID	proportional-integral-derivative
PLFRAME	physical layer frame
QPSK	quadrature phase shift keying
PLL	phase-locked loop
RF	radio frequencies
SER	switch-error rate
SES	Société Européenne des Satellites
SFRAME	super frame
SMF	single mode fiber
SNR	signal-to-noise ratio
SOA	semiconductor optical amplifier
SOF	start of frame
SOSF	start of super frame
TDMA	time division multiple access
TS	transport stream
VPDL	variable photonic delay line